

Special Section:

Recent Progresses in Oceanography and Air-Sea Interactions in Southeast Asian Archipelago

Key Points:

- We report the first data set of carbonate system parameters in the western Indonesian Seas
- While physical processes exerted large controls on the carbonate dynamics, significant DIC removal was observed in the upper Sunda Strait

Correspondence to:M. Dai,
mdai@xmu.edu.cn**Citation:**

Hamzah, F., Agustadi, T., Susanto, R. D., Wei, Z., Guo, L., Cao, Z., & Dai, M. (2020). Dynamics of the Carbonate System in the Western Indonesian Seas During the Southeast Monsoon. *Journal of Geophysical Research: Oceans*, 125, e2018JC014912. <https://doi.org/10.1029/2018JC014912>

Received 4 JAN 2019

Accepted 18 DEC 2019

Accepted article online 4 JAN 2020

Dynamics of the Carbonate System in the Western Indonesian Seas During the Southeast Monsoon

Faisal Hamzah^{1,2}, Teguh Agustadi², R. Dwi Susanto^{3,4}, Zexun Wei^{5,6}, Liguu Guo¹, Zhimian Cao¹, and Minhan Dai¹

¹State Key Laboratory of Marine Environmental Science and College of Ocean and Earth Science, Xiamen University, Xiamen, China, ²Ministry of Marine Affairs and Fisheries, Institute for Marine Research and Observation, Bali, Indonesia, ³Department of Atmospheric and Oceanic Science, University of Maryland, MD, USA, ⁴Faculty of Earth Science and Technology, Bandung Institute of Technology, Bandung, Indonesia, ⁵Ministry of Natural Resources of China, First Institute of Oceanography, Qingdao, China, ⁶Laboratory for Regional Oceanography and Numerical Modeling, Qingdao National Laboratory for Marine Science and Technology, Qingdao, China

Abstract We present a unique water column data set of dissolved inorganic carbon (DIC) and total alkalinity (TALK) from a cruise to the western Indonesian Seas during the southeast monsoon, covering the Karimata Strait, western Java Sea, and Sunda Strait. Salinity-normalized TALK (NTALK) in the surface water ranged 2,297–2,348 $\mu\text{mol kg}^{-1}$, very close to typical values observed in the tropical ocean. In the Karimata Strait, the Kapuas River plume was observed, featuring low salinity, DIC, and TALK. In the western Java Sea, where waters were well mixed, we observed relatively homogeneous distributions of salinity, DIC, and TALK. In the Sunda Strait, waters intruding from the Java Sea occupied the upper layer, and below was the Indian Ocean water with lower values of salinity, DIC, and TALK. In its deep portion, depth profiles of normalized DIC and NTALK were very similar to those observed in the Indian Ocean. Physical processes and air-sea gas exchange exerted predominant controls on the carbonate system in the Karimata Strait and western Java Sea. While both processes play large roles in the Sunda Strait, a net DIC removal of $31 \pm 23 \mu\text{mol kg}^{-1}$ in the surface mixed layer were revealed. The drawdown of DIC is consistent with an overall supersaturation of dissolved oxygen (102–107%), suggesting significant organic carbon production. In the subsurface-intermediate waters of the Sunda Strait mainly influenced by the advection of Indian Ocean water, a net DIC consumption of $54 \pm 45 \mu\text{mol kg}^{-1}$ was distinct, likely stimulated by the nutrients supplied from the Indian Ocean.

Plain Language Summary Research on the carbonate system in the tropical regime of the Indonesian Seas is minimal, which hampers our understanding to its essential role in interbasin exchanges of material and energy via the Indonesian throughflow. Here we present a unique data set to examine the dynamics of the carbonate system in the western Indonesian Seas. Based on DIC and TALK relationships, we show that water mass mixing in the western Indonesian Seas during the southeast monsoon is dominated by zonal wind-mixed waters from the plume of the Kapuas River, the Java Sea and South China Sea mixed water, and the subsurface Indian Ocean water. These processes resulted in homogenous distributions of physical properties and carbonate system parameters. However, biologically mediated DIC consumption occurred in the surface mixed layer of the Sunda Strait, which led to an increase in dissolved oxygen saturation, the saturation state of aragonite (Ω_{arag}), and pH. Overall, our region was a source of atmospheric CO_2 as previously reported, although the controlling processes may vary with respect to time at both seasonal and interannual timescales.

1. Introduction

Located between two major ocean basins, the Pacific and Indian Oceans, the Indonesian Seas are the only low-latitude interbasin pathway; known as the Indonesian throughflow (ITF), they are an essential component of the earth's climate system (Gordon, 1986; Wyrski, 1961). As part of thermohaline circulation, the ITF has received much attention, largely due to its vitally important role in the transport of mass, heat, and freshwater (Broecker, 1991; Gordon, 1986, 2005; Gordon et al., 2003; Hirst & Godfrey, 1993; Schneider, 1998; Sprintall et al., 2014; Wajsowicz & Schneider, 2001; Wijffels et al., 1992). However, the general biogeochemistry of the Indonesian Seas and their role in the global carbon cycle remain largely unknown, despite emerging research efforts across multiple fields. This knowledge gap is in striking contrast to the importance

of the Indonesian Seas to global marine ecosystems. It is well-known that, as part of the coral triangle, the Indonesian Seas have the richest abundance of coral reefs in the world, covering a total area of 51,020 km² (Tun et al., 2004). Understanding the dynamics of the carbonate system in this region is a prerequisite to meet the challenges of this vulnerable ecosystem and similar coastal tropical environments under ongoing ocean warming and acidification (Baker et al., 2008; Ilyina et al., 2009).

Kartadikaria et al. (2015) reported that both the inlet and outlet of the ITF are appreciable CO₂ sinks, while the Makassar Strait (a main route of the ITF) features highly dynamic air-sea CO₂ exchanges associated with water mass mixing between buoyant, freshened Java Sea water (JSW) and the Pacific. These authors also showed that the Indonesian archipelago acts as a source of CO₂ to the atmosphere, with an air-sea flux of 3.7 ± 2.2 mol m⁻² year⁻¹ during the austral summer season. Similar results were also reported by Afdal et al. (2012), showing that the Gaspar Strait near Belitung Island is a source of atmospheric CO₂, with fluxes ranging from 0.35–1.16 mol m⁻² year⁻¹.

Controls on the CO₂ system in the Indonesian Seas are, however, largely unknown due to the complex physical and biogeochemical processes involved. Furthermore, the Indonesian Seas carbonate system as an essential component of the global CO₂ system is even less understood. In this study, we present a unique water column data set of carbonate system parameters from the western Indonesian Seas during the southeast monsoon, covering three contrasting regimes with different degrees of water mass mixing and riverine inputs. We sought to present the dynamics of the regional carbonate system and diagnose the controls exerted by both physical water mass mixing and biological alteration. Additionally, we assessed the saturation state of calcium carbonate in order to provide baseline information of ocean acidification, which has a particular significance to the regional ecosystem.

2. Materials and Methods

2.1. Study Area

The western Indonesian Seas are part of the Sunda Shelf and connected to the South China Sea (SCS) in the north through the Karimata Strait and the Indian Ocean in the south via the Sunda Strait (Figure 1b). The Karimata Strait is located between Sumatra and Kalimantan Island, has shallow water depths of <40 m, and contains three main islands: Bangka, Belitung, and Serutu (Figure 1c). The western Java Sea is characterized by shallow water depths of 20–30 m (Figure 1d) and is a main passage for both JSW and the SCS through-flow, with reversals in circulation during boreal summer (Figure 1b blue pathway—from the Java Sea to the SCS) and winter (Figure 1b magenta pathway—from the SCS to the Java Sea; Fang et al., 2010; He et al., 2015; Susanto et al., 2013). The SCS throughflow is an important branch of the ITF and is also known as the SCS-Indonesian Seas Transport Exchange (Susanto et al., 2010). Located between Java and Sumatra, the Sunda Strait consists of several islands and is an important passage connecting the Java Sea and the Indian Ocean (Figure 1e; Potemra et al., 2016; Putri, 2005; Susanto et al., 2016). The narrowest part of the passage is only 10- to 24-km wide and has irregular bottom topography (Potemra et al., 2016; Wyrтки, 1961), widens to ~35 m near the western Java Sea, and is up to ~50-km wide near the Indian Ocean where water depths reach 900 m (Putri, 2005).

The western region of the Indonesian Seas is dominated by low salinity water and shallow water depths. Numerous rivers empty into the Java Sea, such as the Kapuas River (Kalimantan Island) and Way Sekampung from Sumatra, and the Ciujung, Citarum, Ciliwung, and Cisadane from Java, with a total discharge from all rivers of 47.6×10^3 m³ s⁻¹ (long-term average between 2005 and 2015; Kästner et al., 2018; <http://www.pusair-pu.go.id/>; Figures 1b and 2). As a consequence, the Java Sea features low salinities (<32 practical salinity unit [PSU]) throughout the entire water column, accompanied by high nutrient supplies coinciding with large amounts of rainfall (Wyrтки, 1961).

Our study area is also strongly influenced by the local climate of the Asia-Australia monsoon system (Potemra et al., 2016; Saji et al., 1999; Susanto et al., 2001; Susanto et al., 2006; Susanto et al., 2016; Susanto & Marra, 2005) with the Asian, or northwest monsoon present from December to February, and the Australian, or southeast monsoon present from June to August. From March to May and from September to November are the transitional periods (Aldrian & Susanto, 2003). During the northwest monsoon, low salinity, warm water flows from the SCS into the Java Sea via the Karimata Strait

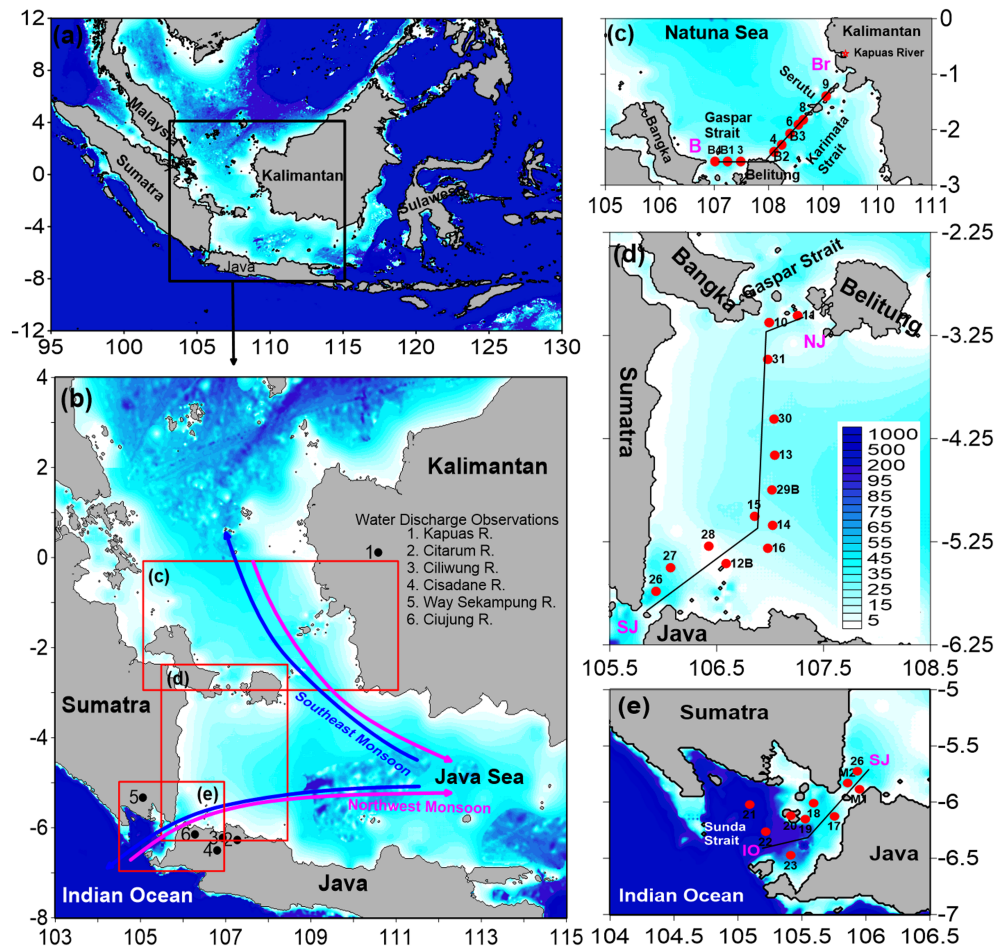


Figure 1. Maps of the western Indonesian seas. The black box shows the study area of a cruise during the southeast monsoon season in June 2015 (a). Red rectangles in panel (b) denote three subregions: the Karimata Strait (c), western Java Sea (d), and the Sunda Strait (e). Black lines in panels (c), (d), and (e) indicate cruise transects, and the red dots show stations where physical and carbonate parameters were obtained. Blue and magenta arrows in panel (b) denote the throughflow from the Java Sea to the South China Sea and the Indian Ocean and its reversal during the southeast monsoon (SEM) and northwest monsoon (NWM), respectively. Isobath values (shown by blue shading) in panels (c), (d), and (e) are in meters.

(Figures 3a and 4a, Fang et al., 2010; Susanto et al., 2013; Wang et al., 2019; Wei et al., 2019). Water transport through this strait is southward at 2.7 ± 1.1 Sv ($1 \text{ Sv} = 10^6 \text{ m}^3 \text{ s}^{-1}$) during the northwest monsoon (magenta pathway—Figure 1b) and 1.2 ± 0.6 Sv during the southeast monsoon/boreal summer (blue pathway—Figure 1b) (Fang et al., 2010; Susanto et al., 2013). The zonal wind intensifies towards the western Indonesian Seas during the March to May monsoon transition when the northeasterly wind still exists, resulting in inconsistent wind and current patterns. During this period, JSW intrudes into the Indian Ocean with current speeds between 0.2 and 0.4 m s^{-1} (Figure 4b). During the southeast monsoon (June to August), the wind blows northwesterly, drawing waters from the Makassar Strait and Flores Sea into the Java Sea; the low salinity, low-density JSWs flow both into the Indian Ocean and the SCS (Hendiarti et al., 2002; Hendiarti et al., 2005; Potemra et al., 2016; Susanto et al., 2016; Xu et al., 2018). However, in the Karimata Strait, the upper water layer flows towards the SCS while the lower layer current remains flowing south into the Sunda Strait (Figure 4c). As a consequence, the SCS-Indonesian Seas Transport Exchange flow is lower during the southeast monsoon compared to the northwest monsoon (Susanto et al., 2013; Wang et al., 2019; Wei et al., 2019). Transport across the Sunda Strait during the southeast monsoon/boreal summer (blue pathway—Figure 1b) ranges from 0.7 to 0.83 ± 0.20 Sv (Putri, 2005; Susanto et al., 2016), and is 0.24 ± 0.10 Sv during the northwest monsoon/boreal winter (magenta pathway—Figure 1b; Susanto et al., 2016). It is also of great importance that off the Sunda Strait and southern Java is the center of the eastern pole of the Indian Ocean Dipole (10°S to 0°N and 90°E to 110°E), and during

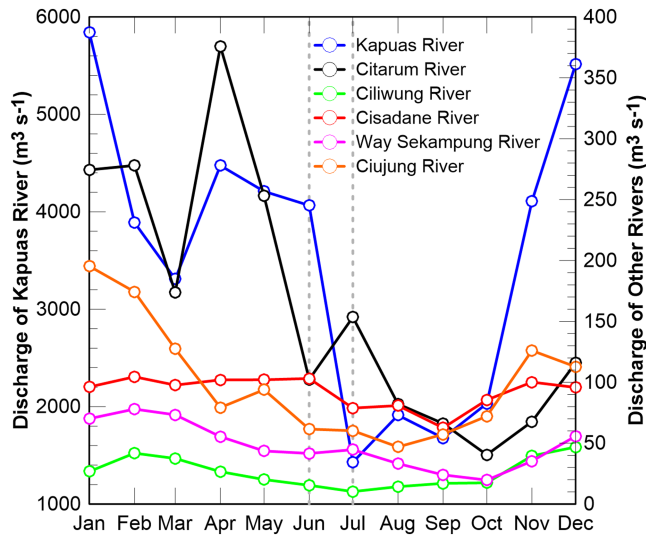


Figure 2. Monthly averages of water discharge from the six largest rivers within the study area from 2005 to 2015. The grey dashed lines in June and July denote the timing of cruise observations. Kapuas River discharge data are from Kästner et al. (2018), and data for the other rivers are from the Research and Development Center for Water Resources, Ministry of Public Works and Housing, Indonesia (<http://www.pusair-pu.go.id/>).

positive Indian Ocean Dipole events, low salinity water from the Java Sea significantly affects sea surface temperature and upwelling along the southern coast of Java-Sumatra (Saji et al., 1999; Setiawan et al., 2015; Susanto et al., 2016; Xu et al., 2018; Xue et al., 2016).

2.2. Sampling and Analyses

Our observations were conducted during the southeast monsoon from 8 to 15 June 2015 onboard the R/V Baruna Jaya VIII (Indonesian Institute of Sciences), covering three different subregions of the western Indonesian Seas: the Karimata Strait, the western Java Sea, and the Sunda Strait (Figures 1c–1e). During the cruise, we measured salinity, temperature, dissolved oxygen (DO), and carbonate system parameters. Water samples for dissolved inorganic carbon (DIC), total alkalinity (TALK), and DO were collected from 12-L Niskin bottles attached to a rosette system.

Samples for DO analysis were collected in 60-ml biological oxygen demand bottles and treated with 0.5 ml of $MnCl_2$ and 0.5 ml of NaOH-KI. The samples were then immersed in a thermostat ($25.0^\circ C$) for ~ 2 hr before onboard analysis. Samples for both DIC and TALK were taken and stored in 250-ml borosilicate glass bottles and poisoned using saturated $HgCl_2$. The samples were stored in the dark and sent to the State Key Laboratory of Marine Environmental Science, Xiamen University, China for detailed

analysis. We followed the protocol of best practices for measuring ocean carbonate system parameters on samples collected for DIC and TALK (Cao et al., 2011; Dickson et al., 2007).

Temperature and salinity were recorded shipboard with a calibrated SBE-19-plus Conductivity-Temperature-Depth recorder (Sea-Bird® 911 plus). A spectrophotometric method was used to determine DO concentrations onboard (Jiang et al., 2011; Labasque et al., 2004; Pai et al., 1993) with a precision of $\pm 1.25\%$. For DIC and TALK analyses, samples were immersed in a thermostatic bath with a temperature maintained at $25.0 \pm 0.1^\circ C$. DIC was determined by acidifying seawater with phosphoric acid (H_3PO_4) and quantifying the released CO_2 with a nondispersive infrared detector (Li-Cor® 7000) using an Apollo SciTech model AS-C3 DIC Analyzer. After DIC analysis, the remaining sample was used for TALK measurements. TALK was determined by open cell Gran titration with hydrochloric acid (HCl) on 25 ml of sample using a KloeHN digital syringe pump (Apollo SciTech model AS-ALK1+). Both DIC and TALK measurements had a precision of $\pm 2 \mu mol kg^{-1}$ (Cao et al., 2011). DIC and TALK were calibrated against certified reference material provided by Dr Andrew G. Dickson of the Scripps Institution of Oceanography. pH, the partial pressure of CO_2 (pCO_2) and aragonite saturation state (Ω_{arag}) were calculated using the CO_2SYS program (Lewis & Wallace, 1998); the coefficients for the CO_2 system were from Mehrbach et al. (1973) as refitted by Dickson and Millero (1987). Normalized DIC (NDIC) and TALK (NTALK) values were calculated relative to open ocean salinity (Chen & Millero, 1979; Chen & Pytkowicz, 1979) following equation (1):

$$NP = \frac{P^{obs}}{S^{obs}} \times S^{ref}. \quad (1)$$

where NP is the normalized TALK or DIC value, P^{obs} is the measured value, S^{obs} is the measured salinity, and S^{ref} is the average salinity of the ocean (35 PSU).

The air-sea CO_2 flux (F_{CO_2}) between the surface water and the atmosphere was determined as follows:

$$F_{CO_2} = k \times s \times \Delta pCO_2, \quad (2)$$

where k is gas transfer velocity, s is the solubility of CO_2 (Weiss, 1974), and ΔpCO_2 is the pCO_2 difference between the surface water and the atmosphere. The empirical functions in Sweeney et al. (2007) and Ho et al. (2006) were used for gas transfer velocity parameterization using the following formula:

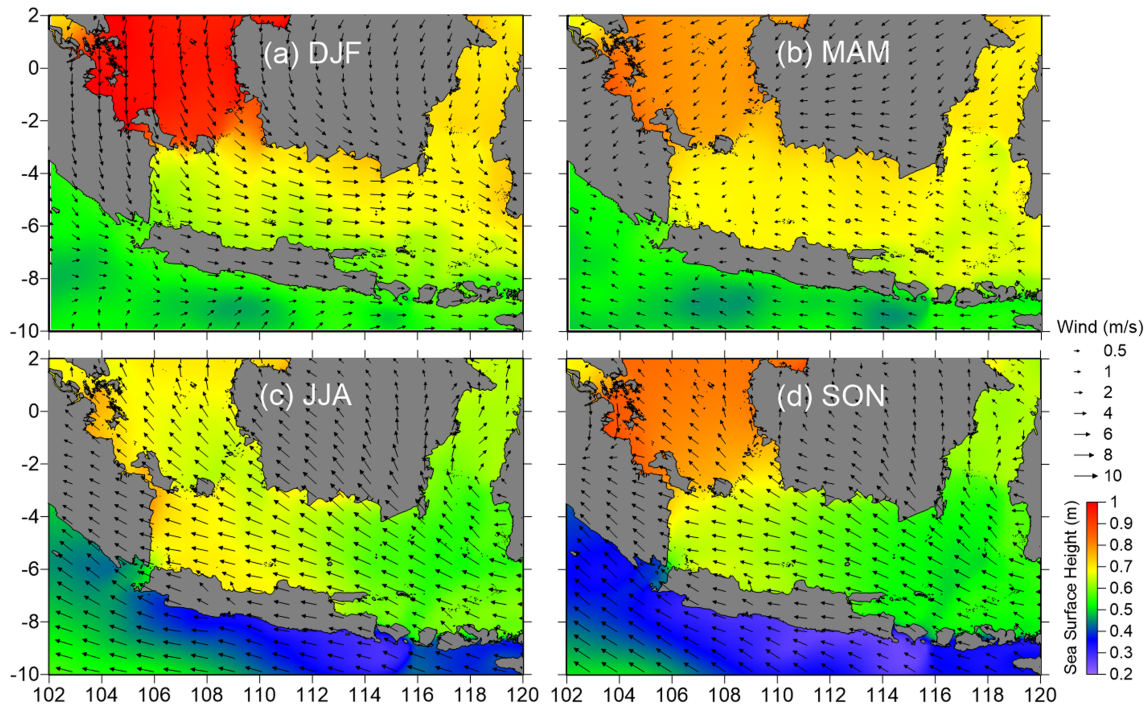


Figure 3. Long-term seasonal averages of sea surface heights (m) with superimposed winds (m/s) over the region of the Indonesian Seas (10°S-2°N and 102°E-120°E). (a-d) Representation map for the DJF, MAM, JJA, and SON seasons. Sea surface height dataset is obtained from model results by the Infrastructure Development of Space Oceanography (INDES0) project (Tranchant et al., 2016). The INDES0 data are obtained from http://www.indeso.web.id/indeso_wp/index.php/en/, while the wind dataset is used and downloaded from <https://coastwatch.pfeg.noaa.gov/erddap/index.html>. DJF, December to February; JJA, June to August; MAM, March to May; SON, September to November.

$$k = 0.27 \times U_{10}^2 \times (Sc/660)^{-0.5} \quad (3)$$

where U_{10} and Sc are the wind speed at 10 m above sea level and the Schmidt number at the in situ temperature in the seawater (Wanninkhof, 1992). Daily wind data were obtained from <https://coastwatch.pfeg.noaa.gov/erddap/griddap/>. Atmospheric pCO_2 was determined from the atmospheric CO_2 fraction (χCO_2) at the Bukit Kota Tabang station, West Sumatera, Indonesia and the barometric pressure (P) after correcting for water vapor pressure (P_{H_2O}) (Weiss & Price, 1980):

$$pCO_2^{atm} = (P - P_{H_2O}) \times \chi CO_2 \quad (4)$$

The average air χCO_2 during the June 2015 cruise (395.85 ppm) was used in the calculation and obtained from National Oceanic and Atmospheric Administration/Earth System Research Laboratory (<https://www.esrl.noaa.gov/gmd/>) at the Bukit Kota Tabang station, West Sumatera, Indonesia. Positive F_{CO_2} values indicate the evasion of CO_2 to the atmosphere and negative values suggest an oceanic sink for atmospheric CO_2 .

3. Results

3.1. Hydrographic Characteristics

The potential temperature-salinity diagram is shown in Figure 5. The warm, homogeneous water in the near-surface layer along a salinity gradient 31 to 33 PSU, with temperatures of $\sim 30^\circ C$ and a potential density (σ_θ) of 19–20.25 $kg\ m^{-3}$, is indicative of mixing between SCS water, the Kapuas River plume, and JSW (hereafter). JSW intruded into the Sunda Strait, appearing in the upper 40 m mixed with surface Indian Ocean water along $\sigma_\theta = \sim 20.4\ kg\ m^{-3}$. Beneath this layer was North Indian Subtropical Water, featuring a salinity maximum of ~ 35.01 PSU, a σ_θ of ~ 21 to 25 $kg\ m^{-3}$, and significant variations in temperature which gradually declined from $27^\circ C$ to $18^\circ C$ with depth. At intermediate depths, the salinity minimum was found along a σ_θ

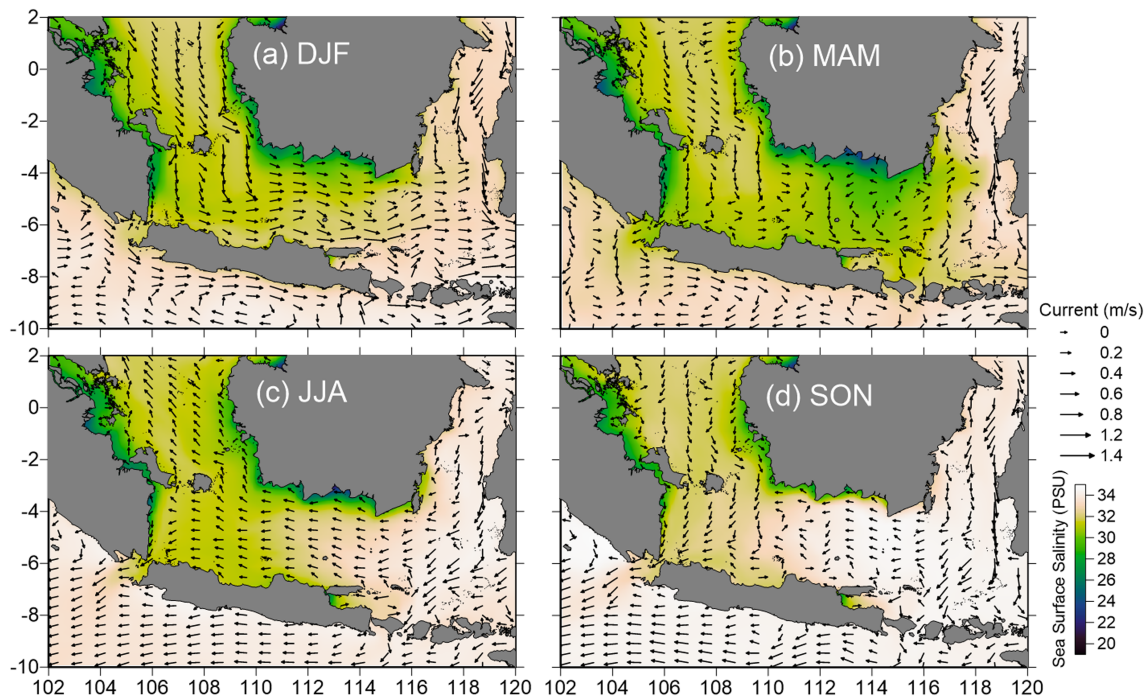


Figure 4. Long-term seasonal averages of salinities (PSU) with superimposed currents (m/s) over the region of the Indonesian Seas (10°S-2°N and 102°E-120°E). (a–d) Representation map for the DJF, MAM, JJA, and SON seasons. Current and salinity (0 to 20-m depth averaged) data sets are obtained from model results by the Infrastructure Development of Space Oceanography (INDES0) project (Tranchant et al., 2016). The INDES0 data are obtained from http://www.indeso.web.id/indeso_wp/index.php/en/. PSU, practical salinity unit; DJF, December to February; JJA, June to August; MAM, March to May; SON, September to November.

of $\sim 26.3 \text{ kg m}^{-3}$ and a temperature of 13°C , representing North Indian intermediate water. At deeper layers with a relatively constant σ_θ of $\sim 27.5 \text{ kg m}^{-3}$, salinity and temperature were ~ 34.7 PSU and $\sim 6^\circ\text{C}$, respectively, indicative of upper Indian Ocean Deep Water. The similarity in water mass structure with that of the major ITF outflow passages of the Lombok Strait and the southern coast of Java-Bali (Atmadipoera et al., 2009), along with time-series measurements of velocity in the Sunda Strait (Susanto et al., 2016), confirm that the Sunda Strait is one of the exit passages of the ITF into the Indian Ocean, as previously reported (Susanto et al., 2016; Xu et al., 2018).

Surface distributions of salinity and temperature are shown in Figures 6a and 6b. During the survey period under the early southeast monsoon, the Kapuas River plume water, with a low salinity (~ 31.31 PSU) and a relatively high temperature ($\sim 29.87^\circ\text{C}$), was clearly seen near Kalimantan in the Karimata Strait. In the Gaspar Strait, away from the plume, we observed a higher salinity (~ 32.98 PSU) but similar temperatures. The water in the western Java Sea was warm ($29.5\text{--}29.9^\circ\text{C}$) and had a low salinity of ~ 32.53 PSU due to local riverine runoff into the region. In the Sunda Strait, surface salinity values were low and homogeneous (averaging ~ 32.88 PSU), the lowest of which was found at the M2 Sunda Strait station (~ 31.41 PSU), suggesting additional freshwater input from rivers on Sumatra and the Java Islands.

Vertical profiles of salinity and temperature across the Karimata Strait and along the western Java Sea and the Sunda Strait are shown in Figures 7a and 7b. The eastern Karimata Strait was characterized by a lower salinity (31.40 PSU), affected by the plume of the Kapuas River. The plume is about $\sim 17\text{-m}$ thick and spread across ~ 70 km in the center of the strait. In contrast, at the western portion of the Karimata Strait, the salinity was slightly higher (~ 32.98 PSU) and homogeneous until 35-m depth due to strong monsoon winds and less influence from the river plume. Similarly, water in the western Java Sea had homogeneous salinities (32.6–33.0 PSU) due to strong zonal monsoon winds and shallow water depths. In the Sunda Strait, it was clear that intrusion of JSW occurred in the upper $\sim 30\text{- to }50\text{-m}$ layer. Salinity in this layer was low (32.50–33.50 PSU), while in the subsurface layer in up to $\sim 80\text{--}130$ m water depth the salinity was higher (34.64–35.01 PSU), occupied by Indian Ocean water.

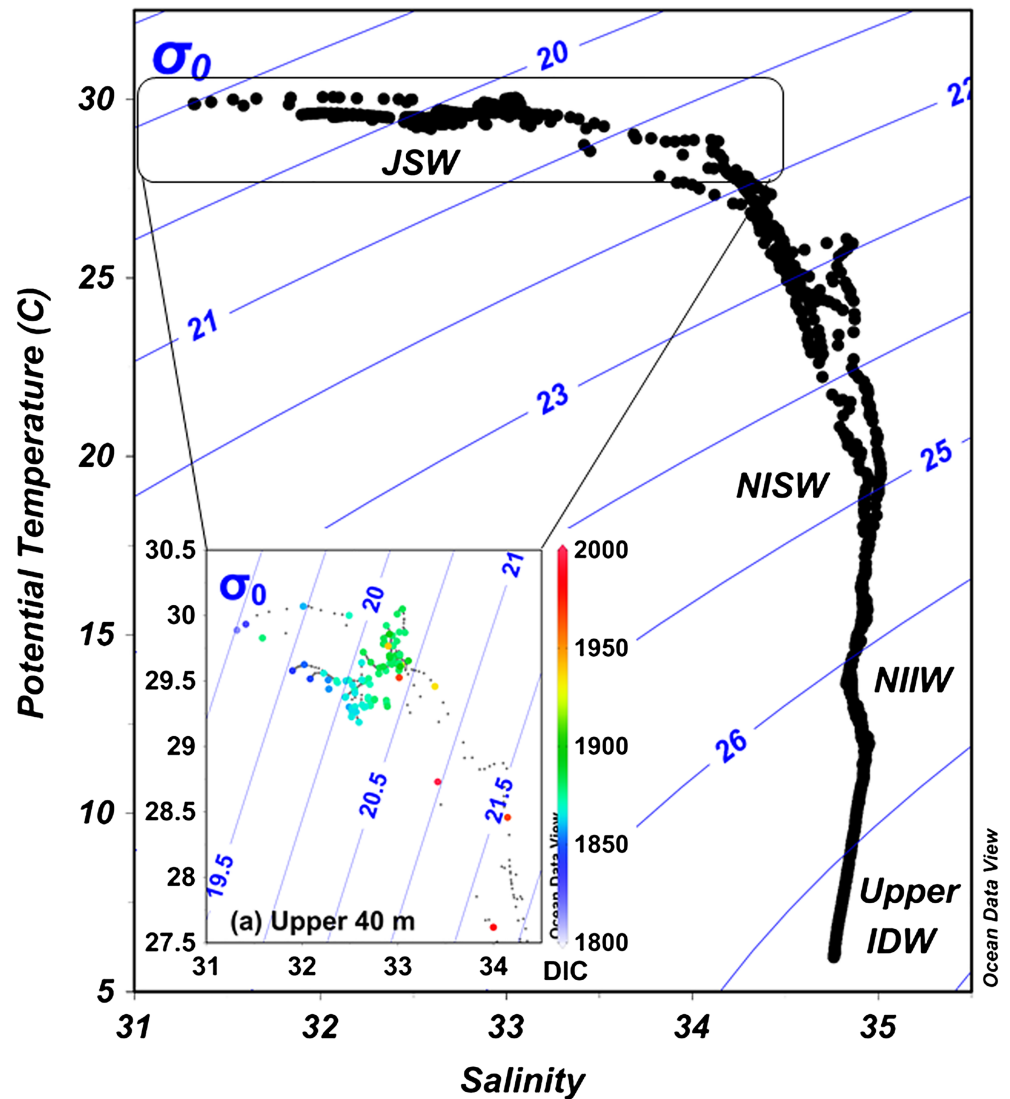


Figure 5. Potential temperature versus salinity diagram showing water mass characteristics in the western Indonesian Seas during June 2015. The water mass in the study area consists of Java Sea water (JSW), North Indian subsurface water (NISW), North Indian intermediate water (NIIW), and upper North Indian deep water (IDW). The data were obtained from surface water at all stations, to a maximum depth of 900 m at station 21. The inserted panel (a) shows water mass mixing in the upper 40 m of the water column with dissolved inorganic carbon (DIC) concentrations superimposed. Ocean Data View software (<http://odv.awi.de>, Schlitzer, 2018) was used to create the figure.

3.2. Distributions of Carbonate System Parameters

The surface distributions of carbonate parameters are displayed in Figures 6c–6f. DIC and TALK ranged from 1,814–1,895 $\mu\text{mol kg}^{-1}$ and 2,066–2,188 $\mu\text{mol kg}^{-1}$, respectively. The distribution of TALK was generally similar to salinity, as was the distribution of DIC, with the exception of the western Java Sea where lower DIC was found at both Sta. 27 (2,078 $\mu\text{mol kg}^{-1}$) and Sta. 31 (2,089 $\mu\text{mol kg}^{-1}$). In the Karimata Strait, DIC and TALK had similar patterns with lower concentrations near the Kapuas River (DIC = 1,814 $\mu\text{mol kg}^{-1}$ and TALK = 2,066 $\mu\text{mol kg}^{-1}$).

Vertically, buoyant waters in the top 17 m of the eastern Karimata Strait were accompanied by low DIC ($\sim 1,814 \mu\text{mol kg}^{-1}$) and TALK ($\sim 2,066 \mu\text{mol kg}^{-1}$; Figures 7c–7d). Beneath this buoyant freshwater as far west as Bangka Island (Sta. B4), the concentrations of DIC and TALK increased, reaching $\sim 1,882 \mu\text{mol kg}^{-1}$ and $\sim 2,178 \mu\text{mol kg}^{-1}$, respectively. In the western Java Sea, DIC and TALK were homogeneous, with slightly lower concentrations near Jakarta Bay and Seribu Island, suggesting biological uptake of

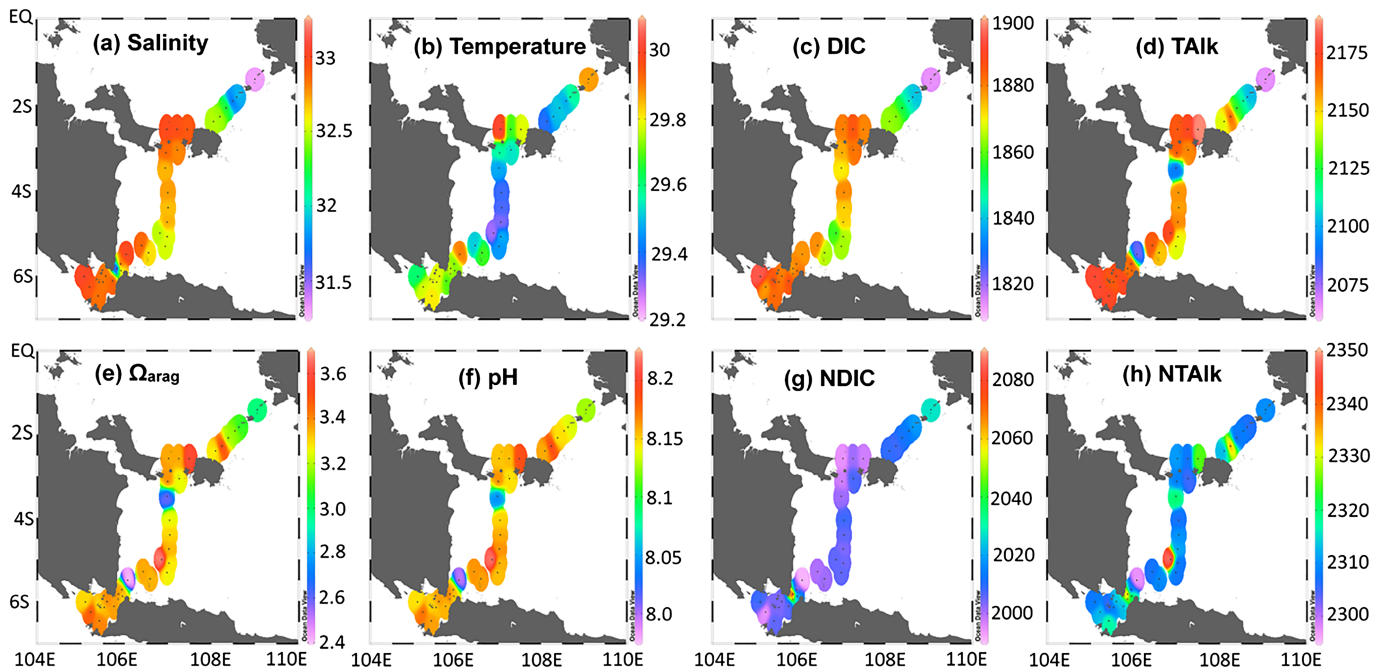


Figure 6. Surface distributions of (a) salinity (PSU), (b) temperature ($^{\circ}\text{C}$), (c) dissolved inorganic carbon (DIC, $\mu\text{mol kg}^{-1}$), (d) total alkalinity (TALK, $\mu\text{mol kg}^{-1}$), (e) aragonite saturation state (Ω_{arag}), (f) pH, (g) NDIC ($\mu\text{mol kg}^{-1}$), and (h) NTalk ($\mu\text{mol kg}^{-1}$) in the western Indonesian Seas during June 2015. The data in the panels were obtained from a depth of 5 m. NDIC, normalized dissolved inorganic carbon; NTalk, normalized total alkalinity.

DIC (see discussion in section 4.2). The distributions of DIC and TALK in the Sunda Strait gradually increased with depth, with values ranging from 1,880 to 2,057 $\mu\text{mol kg}^{-1}$ and from 2,100 to 2,200 $\mu\text{mol kg}^{-1}$, respectively. Indian Ocean water brought high levels of DIC and TALK and mixed with JSW in the center of the strait at Sta. 17 (see cross section of salinity, TALK, and DIC in Figures 1 and 7). Comparing the surface layers of the Sunda Strait, our measurements were more consistent than those off the southern coast of Java (DIC = 1,884–1,973 $\mu\text{mol kg}^{-1}$ and TALK = 2,189–2,240 $\mu\text{mol kg}^{-1}$; Xue et al., 2016) and in the southern SCS (DIC = 1,895–1,908 $\mu\text{mol kg}^{-1}$ and TALK = 2,196–2,206 $\mu\text{mol kg}^{-1}$) and slightly lower than those in the Indian Ocean (DIC \sim 1,950 $\mu\text{mol kg}^{-1}$ and TALK \sim 2,250 $\mu\text{mol kg}^{-1}$; Bates et al., 2006).

Surface and vertical distributions of Ω_{arag} and pH were very consistent with DIC, showing low values (\sim 3 and \sim 8.13, respectively; Figures 6e–6f and 7e–7f) across the entire plume of the Kapuas River down to the top of the bottom layer in the center of the strait. In the western Java Sea, both Ω_{arag} and pH were homogeneous except at Stas. 27 and 31 where surface Ω_{arag} values of 2.4 and 2.6 and pH values of 8.00 and 8.04 were recorded, respectively. In the Sunda Strait, both Ω_{arag} and pH gradually decreased with depth, ranging from 3.6 to 1.1 and from 8.18 to 7.89, respectively. Ω_{arag} and pH were slightly lower below the mixed layer ($\Omega_{\text{arag}} \sim$ 2.0 and pH \sim 7.99). In the deeper layer (\sim 900 m), Ω_{arag} values were near saturation (\sim 1.08), and the pH was 7.83.

In order to better compare with other regions, we normalized both TALK and DIC in the study region to a fixed salinity ($S = 35$ PSU), represented as NDIC and NTalk, respectively. Surface NDIC in the region generally ranged from 1,994 to 2,080 $\mu\text{mol kg}^{-1}$ (Figure 6g). Surface NTalk ranged 2,297–2,348 $\mu\text{mol kg}^{-1}$, and the highest value was found in the western Java Sea at Sta. 15 (Figure 6h). Higher NDIC was observed in the plume water of the Kapuas River (average \sim 2032 $\mu\text{mol kg}^{-1}$) and lower NDIC was found in the Gaspar Strait (Figure 7g). The NDIC and NTalk were homogenous in the western Java Sea and are higher than those in the southern SCS (NDIC = 1,962–1,970 $\mu\text{mol kg}^{-1}$; Chen et al., 2006) or those in the Sulu Sea, the Indian Ocean, and western Philippine Seas (Chen et al., 2006) suggesting more decomposition of organic matter in our region.

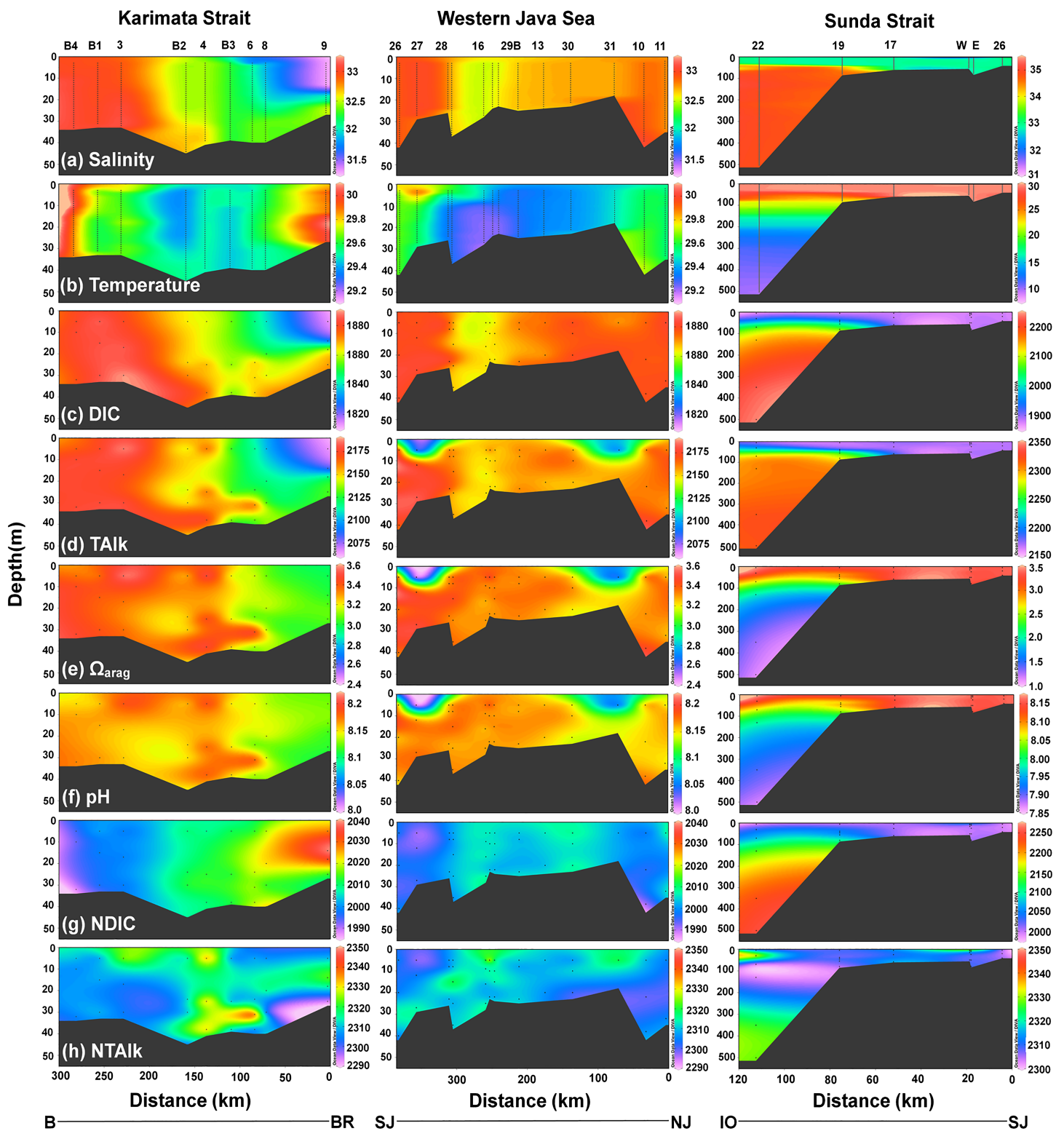


Figure 7. Vertical profiles of (a) salinity (PSU), (b) temperature ($^{\circ}\text{C}$), (c) dissolved inorganic carbon (DIC, $\mu\text{mol kg}^{-1}$), (d) total alkalinity (TALK, $\mu\text{mol kg}^{-1}$), (e) aragonite saturation state (Ω_{arag}), (f) pH, (g) NDIC ($\mu\text{mol kg}^{-1}$), and (h) NTalk ($\mu\text{mol kg}^{-1}$) across the Karimata Strait (left panel; section Borneo [BR]-Bangka Island [B]), along the westernmost portion of the Java Sea (middle panel; section North Java [NJ]-South Java [SJ]), and along the Sunda Strait (right panel; section South Java [SJ]-Indian Ocean [IO]). PSU, practical salinity unit; NDIC, normalized dissolved inorganic carbon; NTalk, normalized total alkalinity.

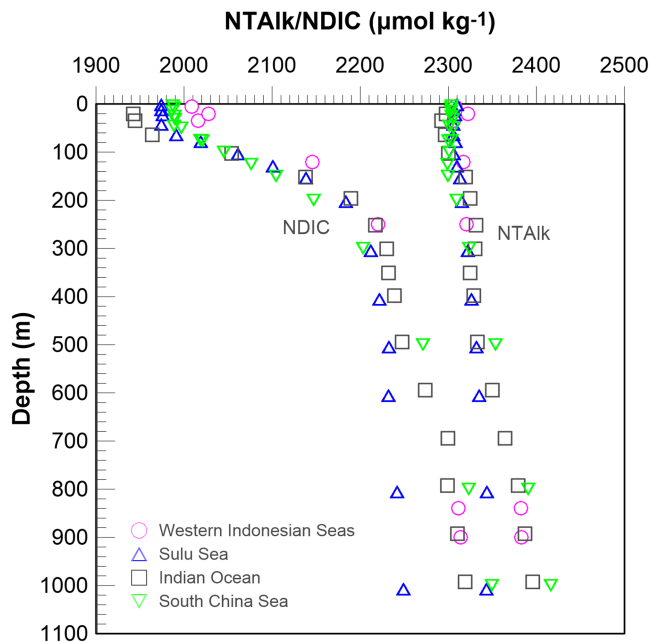


Figure 8. Depth profiles of NDIC and NTalk in the Sunda Strait at station 21 and its comparison with other regions. Dissolved inorganic carbon and total alkalinity data in the Sulu Sea are from Ferrera et al. (2017), from Minhan Dai's Group for the South China Sea, while in the Indian Ocean are from Johnson et al. (2002). NDIC, normalized dissolved inorganic carbon; NTalk, normalized total alkalinity.

Figure 8 shows depth profiles of NDIC and NTalk at a deep station (Sta. 21) in the Sunda Strait. The NDIC and NTalk in the upper 40 m ranged 2,008–2,027 $\mu\text{mol kg}^{-1}$ and 2,306–2322 $\mu\text{mol kg}^{-1}$, respectively. In these layers, NDIC concentration is higher than those observed in the Sulu Sea, the SCS, and the Indian Ocean suggesting more decomposition of organic matter in western Indonesian Seas (Figure 8). These organic matter is likely related to the abundant river input to the region. In the deep water at 300–900 m, NDIC is similar to those in the Indian Ocean but differs from those in the Sulu Sea or in the SCS. NTalk showed homogenous values from the surface layer to 500 m in the western Indonesian Seas, the Sulu Sea, the SCS, and the Indian Ocean. However, at the depth horizon 500–1,000 m, the comparison in NTalk between the Sunda Strait and other regions is similar to that of NDIC.

4. Discussion

4.1. Overview of the Carbonate System During Water Mass Mixing

During our observations, the distributions of carbonate system parameters in the western Indonesian Seas were controlled by mixing of the Kapuas River plume, SCS water, JSW, and Indian Ocean water. We followed the water mass identification approach by Hendiarti et al. (2002) and Atmadipoera et al. (2009) to differentiate typical water mass mixing and distinguish the characteristic source terms of TALK and DIC. During the southeast monsoon, JSW intrudes into the Indian Ocean and becomes well mixed in the Sunda Strait, with DIC versus TALK showing two mixing groups (Figure 9a). The first (Group 1) was between the Karimata Strait, the western Java Sea, and the surface of the Sunda Strait, marked by shallow water depths and westward flow in the Java Sea and southward flow in the Sunda Strait. This mixing group is characterized by low DIC and TALK and high freshwater inputs and predominantly located in the upper 40 m of water along a σ_θ of 20.0 to 20.5 kg m^{-3} but below the plume water which was found along a σ_θ of 19.0 to 20.0 kg m^{-3} (Figure 5a). The mixing was evidenced by the majority of low DIC values ($\sim 1,857$ to $1,967 \mu\text{mol kg}^{-1}$) being scattered across a narrow isopycnal range. The second mixing group (Group 2) was between surface Indian Ocean water, JSW, and upper Indian Ocean Deep Water, including North Indian Subtropical Water and North Indian intermediate water. This water mass is characterized by high DIC and TALK values. All the TALK and DIC values for Group 1 were less than $2,200 \mu\text{mol kg}^{-1}$ and $1,900 \mu\text{mol kg}^{-1}$, respectively. In contrast, TALK values were higher than $2,200 \mu\text{mol kg}^{-1}$, and DIC was higher than $1,900 \mu\text{mol kg}^{-1}$ in mixing Group 2. Some data points fell outside of the TALK-DIC mixing line, indicating that other processes were occurring and resulting in the production and/or removal of TALK and DIC (Figure 9a). The pattern of Group 2 was similar to patterns observed in the southern SCS, with slightly higher TALK and DIC values compared to the Indian Ocean (0 to -15°S and 85°E to 120°E), but lower values than those off the southern coast of Java (Xue et al., 2016).

The distribution of data points along the mixing line (DIC vs. TALK) for Group 2 may vary following monsoon seasons. During the southeast monsoon, seasonal upwelling at the exit of the Sunda Strait (Stas. 21 to 23) was high. Additionally, Hendiarti et al. (2004) and Xu et al. (2018) demonstrated that the discharge of JSW into the Sunda Strait, which features low sea level and sea surface temperature anomalies, enhances primary productivity and results in high levels of chlorophyll-a induced by an increase in the nutrient supply. This suggests high biologically altered DIC through photosynthesis, which is quantitatively analyzed in section 4.2. Comparing our results to the neighboring Indian Ocean and the southern coast of Java (Xue et al., 2016), TALK in the upper 300 m off the southern coast of Java was lower, and DIC values were higher. These carbonate parameters were observed during the upwelling season of the southeast monsoon in September. In the Indian Ocean, however, the data were collected during the winter when downwelling occurs, resulting in both TALK and DIC shifting to higher concentrations in the upper 1,000 m and suggesting the dominant role of physical processes.

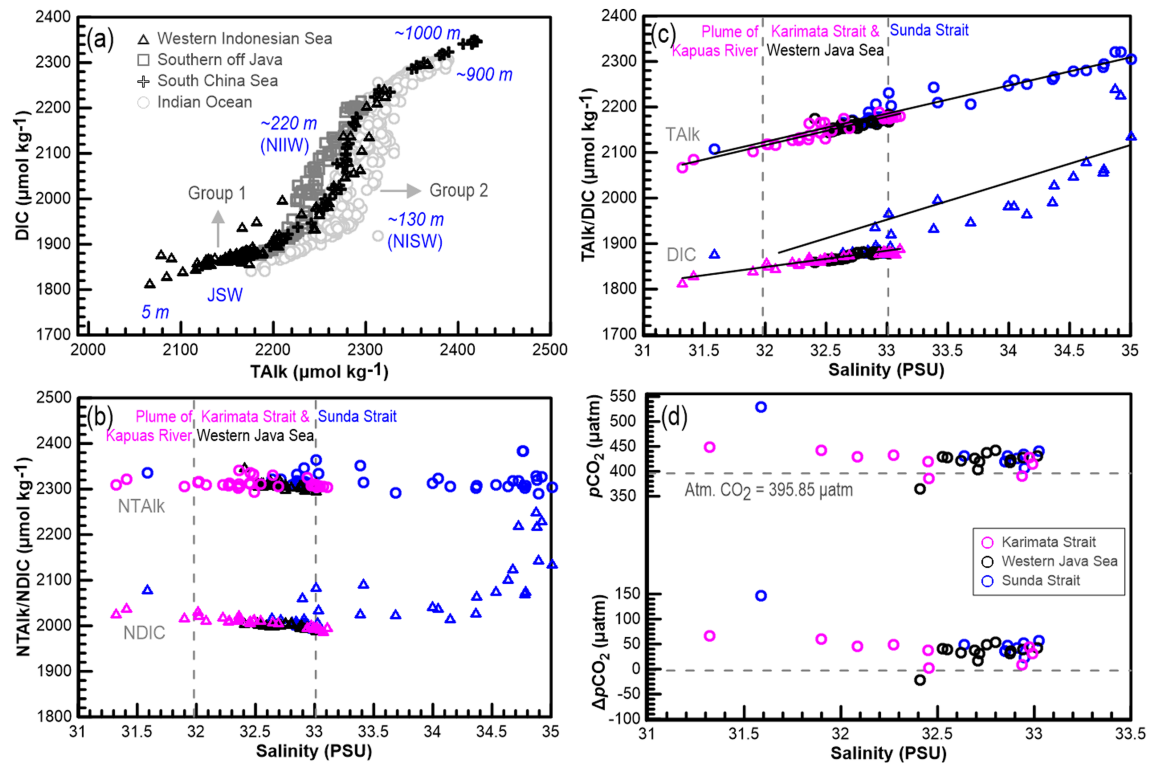


Figure 9. DIC versus TALK across the western Indonesian Seas (triangles) compared to their relationships in the Indian Ocean (circles), southern coast of Java (squares), and southern South China Sea (crosses) (a). The southern coast of Java data set is from Xue et al. (2016), from Minhan Dai's Group for the South China Sea, and the Indian Ocean data set is from the World Ocean Circulation Experiment (WOCE) program (Johnson et al., 2002). Two mixing groups were observed across the study area between plume water and Java Sea water (upper 40 m) and between Java Sea water and upper Indian Ocean Deep water. The numbers in italics symbolize the sampling depth. NTalk versus salinity and NDIC versus salinity throughout the entire water column (b), and DIC versus salinity (triangles) and TALK versus salinity (open circles, $TALK = [66.73 \pm 0.07] * Salinity - [21.44 \pm 5.28]$) relationships in the upper 130 m were also plotted (c). The grey dashed line denotes the different mixing regions based on salinity properties. Surface water partial pressure of carbon dioxide (pCO_2) and the sea-air pCO_2 difference ($\Delta pCO_2 = pCO_2^{seawater} - pCO_2^{air}$) (d). Grey dashed lines in panel (d) denote atmospheric pCO_2 (395.85 μatm) in June 2015. DIC, dissolved inorganic carbon; NDIC, normalized dissolved inorganic carbon; NIIW, North Indian intermediate water; NISW, North Indian subsurface water; JSW, Java Sea water; PSU, practical salinity unit; TALK, total alkalinity; NTALK, normalized total alkalinity.

In the shallower regions, mixing between different water masses showed a reverse transport pattern between surface and subsurface waters in the Karimata Strait and strong intraseasonal and seasonal variability in the Sunda Strait (Fang et al., 2010; Susanto et al., 2013, 2016; Xu et al., 2018). In the Karimata Strait, the plume waters had low DIC and TALK concentrations, with higher concentrations beneath (30–45 m, Figure 10a). We compared this pattern with other stations not affected by the river plume, for example, Sta. 04 in the Karimata Strait and Sta. B1 in the Gaspar Strait, where the water column chemistry was well mixed (Figures 7a and 7d). Such a subsurface pattern is attributable to the southward transport from the SCS to the Java Sea, which brings slightly higher DIC and TALK waters. Indeed, this reversal in transport was clearly seen during the southeast monsoon but disappeared during the northwest monsoon when only southward transport occurs (Fang et al., 2010; Susanto et al., 2013; Wang et al., 2019; Wei et al., 2019). Such southward transport is generated by the wind stress persistently toward the southeast, resulting in a downward sea surface slope from the SCS to the Java Sea allowing water to flow from the surface to depth. These waters could reach the Sunda Strait and the Makassar Strait, which block surface North Pacific waters, thereby changing the volume, heat, and fresh-water transport of the Makassar Strait before exiting to the Indian Ocean, particularly during the northwest monsoon and the monsoon transition periods (see current and salinity patterns in Figure 4). However, in the upper 30 m during the southeast monsoon, low salinity waters with low DIC and TALK are transported northward from the Java Sea to the SCS in an opposite direction to that of the subsurface water. NDIC did not vary in the surface layer and NTALK values were consistent from the surface to the bottom layer, indicating that water mass mixing is a main control.

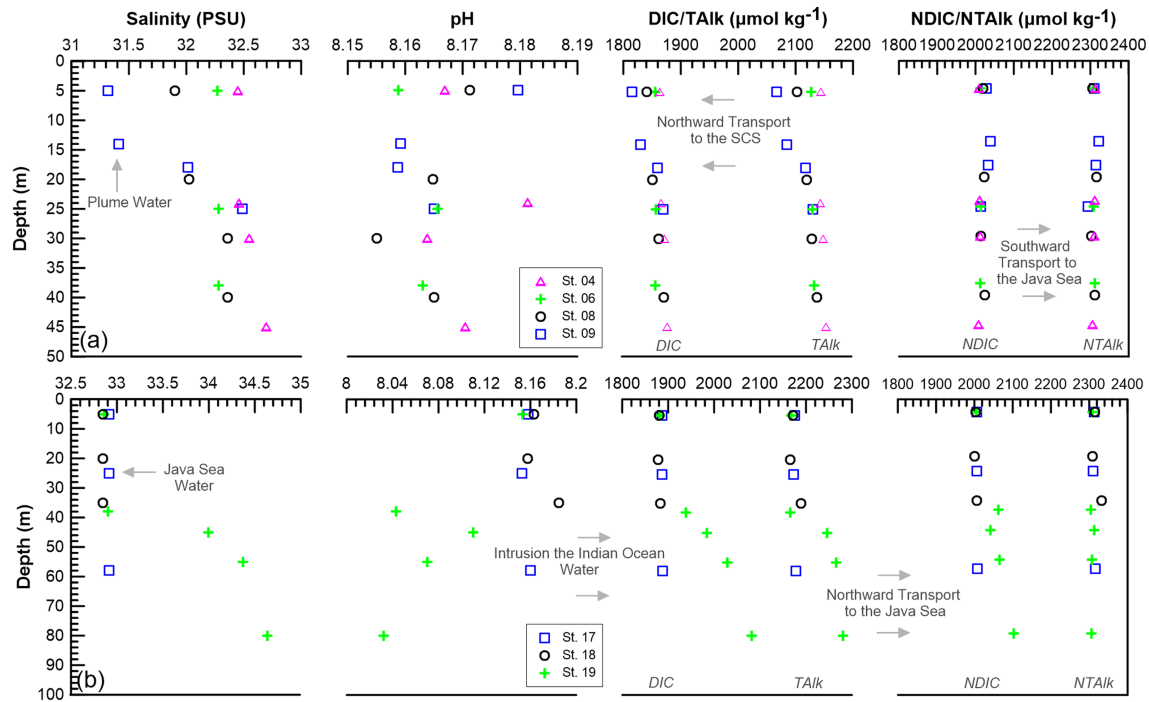


Figure 10. Vertical profiles of salinity (PSU), pH, DIC and Talk ($\mu\text{mol kg}^{-1}$), and NDIC and NTalk ($\mu\text{mol kg}^{-1}$) at stations surrounded by the plume water in (a) the Karimata Strait and (b) the Sunda Strait. PSU, practical salinity unit; DIC, dissolved inorganic carbon; TALK, total alkalinity; NDIC, normalized dissolved inorganic carbon; NTALK, normalized total alkalinity.

In the Sunda Strait, water mass mixing between the fresher and more saline waters showed an obvious effect on DIC and TALK concentrations. The concentrations were similar throughout the entire water column at the strait with a visible influence from JSW (Sta. 17), but the profile changed at Sta. 18 where DIC and TALK values showed higher values beneath 35 m depth (Figure 10b). Indeed, these fresher waters intrude into the Indian Ocean via the Sunda Strait due to continuous wind stress in the western Java Sea, resulting in a different sea level gradient between the Java Sea and southern Sunda Strait (Li et al., 2018; Susanto et al., 2016; Xu et al., 2018). The throughflow would be strongest during the peak of the southeast monsoon, bringing waters with low DIC, TALK, and salinity into the Indian Ocean (Figure 4). Similarly, DIC and TALK concentrations at Sta. 19 were homogenous in the upper ~40 m with slightly higher concentrations beneath, suggesting strong northward transport and injection of Indian Ocean water with high DIC and TALK (Figures 7c–7d). A similar pattern was also observed for NDIC and NTalk values, which were consistently homogenous in the upper layer. The concentrations increased with depth accompanied by a decrease in pH. Xu et al. (2018) suggested that the injection of Indian Ocean water into the Sunda Strait and mixing with JSW is due to Kelvin wave signal penetration from the central Indian Ocean, and upwelling occurs in the southern Sunda Strait due to the intraseasonal surface wind anomalies.

TALK showed a strong correlation with salinity, suggesting that its distribution was largely controlled by physical mixing (Figure 9c). The linear regression of the TALK versus salinity relationship had an intercept of -21.44 ± 5.28 and a slope of 66.73 ± 0.07 . The negligibly low intercept suggests insignificant input of freshwater with zero solutes to the western Indonesian Seas. The slope (66.73) is close to the ratio (65.7) of average TALK ($2,300 \mu\text{mol kg}^{-1}$) to the average salinity (35 PSU) of the surface ocean. The normalized average NTALK in the upper mixed layer (~40 m) was $2,313 \mu\text{mol kg}^{-1}$, which is close to the values observed in the tropical ocean ($2,289\text{--}2,310 \mu\text{mol kg}^{-1}$, Jiang et al., 2014). Note that our measurements ($\text{NTALK} = 2,290\text{--}2,382 \mu\text{mol kg}^{-1}$) from the entire water column of the western Indonesian Seas are slightly lower than those off Sarawak, Sabah, and Brunei Darussalam during the pre-monsoon/Australian transition monsoon (up to $2,430 \mu\text{mol kg}^{-1}$) and post-monsoon/Asian transition monsoon (up to $2,450 \mu\text{mol kg}^{-1}$; Chen, 2002). These differences indicate that TALK in the Sunda shelf is subject to strong seasonal variations.

The observed DIC versus salinity relationship shows that the DIC distribution does not follow conservative mixing behavior, and its concave shape suggests that DIC in the western Indonesian Seas is controlled not only by mixing but also by biological processes, especially in the Sunda Strait (Figure 9c). Another process that might remove DIC is the net evasion of CO₂ to the atmosphere (Guo & Wong, 2015; Tseng et al., 2007). This CO₂ evasion is supported by the fact that the sea-air $p\text{CO}_2$ difference ($\Delta p\text{CO}_2 = p\text{CO}_2^{\text{seawater}} - p\text{CO}_2^{\text{air}}$) across the study area was positive with an average of 44 μatm (Figure 9d). The $\Delta p\text{CO}_2$ across the Karimata Strait, the western Java Sea, and the Sunda Strait ranged 5.55 to 69.18 μatm , -19.80 to 57.45 μatm , and 26.09 to 149.88 μatm , respectively. The strength of sea-air CO₂ flux thus increased towards the plume water of the Kapuas River, with an exception that a highest $\Delta p\text{CO}_2$ of 150 μatm was observed at Sta. M2 (location shown in Figure 1e) in the western Sunda Strait (Figure 9d). CO₂ degassing from the western Indonesian Seas during the southeast monsoon was estimated to be 2.98 $\text{mmol C m}^{-2} \text{day}^{-1}$. This flux is about half of that observed in the western Indonesian Seas during the monsoon transition period in 2011 (Kartadikaria et al., 2015) during a La Niña event that is believed to induce higher CO₂ fluxes with strong wind speeds. Since our study site is very shallow and has strong zonal monsoon winds, we assume that during the mixing process DIC removal through evasion of CO₂ to the atmosphere is rapid.

We can also use a graphical approach based on plots of NTalk against NDIC (Deffeyes diagram, Zeebe & Wolf-Gladrow, 2001) to diagnose the various processes that affect the carbonate system. We show in Figure 11a the NTalk-NDIC diagram using data collected in the upper mixed layer (<40 m). In the Karimata Strait and the western Java Sea, the slope of NTalk-NDIC relationship was slightly positive (0.18 and 0.37), suggesting a mixed control of air-sea CO₂ exchange and CaCO₃ precipitation and dissolution. Net calcification is possible since the study area is surrounded by coral reef ecosystems. The biological alteration of DIC via photosynthesis and respiration was thus minor in both regions. In the Sunda Strait, however, the slope became negative (-0.11), indicating enhanced DIC variations during organic carbon metabolism in addition to the gas exchange.

We took stations 19 to 22 in the Sunda Strait as an example to further demonstrate how DIC dynamics were affected by biological activity, which again showed a negative slope of -0.056 between NTalk and NDIC (Figures 11b and 11c). TALK was mostly conservative against salinity while the majority of DIC data points are below the conservative mixing line (Figure 11c), suggesting net removal of DIC. We calculated the initial NTalk and NDIC of the source water for each field sample, which were constrained by a two end-member mixing scheme (Figure 11c). The initial NTalk values were on average comparable to field observations, suggesting again its conservativity. By comparison, most initial NDIC decreased towards corresponding field values in the Sunda Strait, indicating DIC removal associated with biological production. This is further evidenced by an overall supersaturation of DO in the surface water (Figure 11d). Further quantitative analysis is discussed in section 4.2.

4.2. Quantification of Water Mass Mixing and Biological Alteration in the Upper Mixed Layer

As shown by the vertical salinity, temperature, DIC, and TALK profiles (Figure 7), it is clear that waters in the western Indonesian Seas were well mixed due to the shallow water depths and the strong zonal monsoon winds (Figure 3). During mixing, freshwater inputs from numerous rivers not only diluted the saline water from the SCS and the Pacific Ocean, which intruded via the southern Makassar Strait to the Java Sea (Susanto et al., 2016), but also brought large amounts of nutrients and stimulated primary production. Normalizing TALK (NTalk) to a given salinity resulted in no observable difference in water column profiles, as indicated by their distributions which showed strong physical mixing (Figure 9b). However, some DIC values are below the mixing line (Figure 9c), suggesting high biologically mediated DIC consumption.

To assess biologically mediated DIC (ΔDIC) variations, we first calculated DIC value due to conservative mixing alone, based on a two end-member mixing model. The good positive linear relationship between TALK and salinity (Figure 9c) suggests that waters in the surface mixed layer originated from mixing between rain water and waters beneath the surface mixed layer depth (Cao et al., 2019; Dai et al., 2013). The rain water end-member is determined as a near-zero intercept from TALK versus salinity. Relatively invariable NTalk along salinity gradient (Figure 9b) also points to the presence of the rain water end-member with zero solutes. The conservative-mixing induced DIC and TALK values (DIC^{cons} and $\text{TALK}^{\text{cons}}$) can be calculated according to Dai et al. (2013):

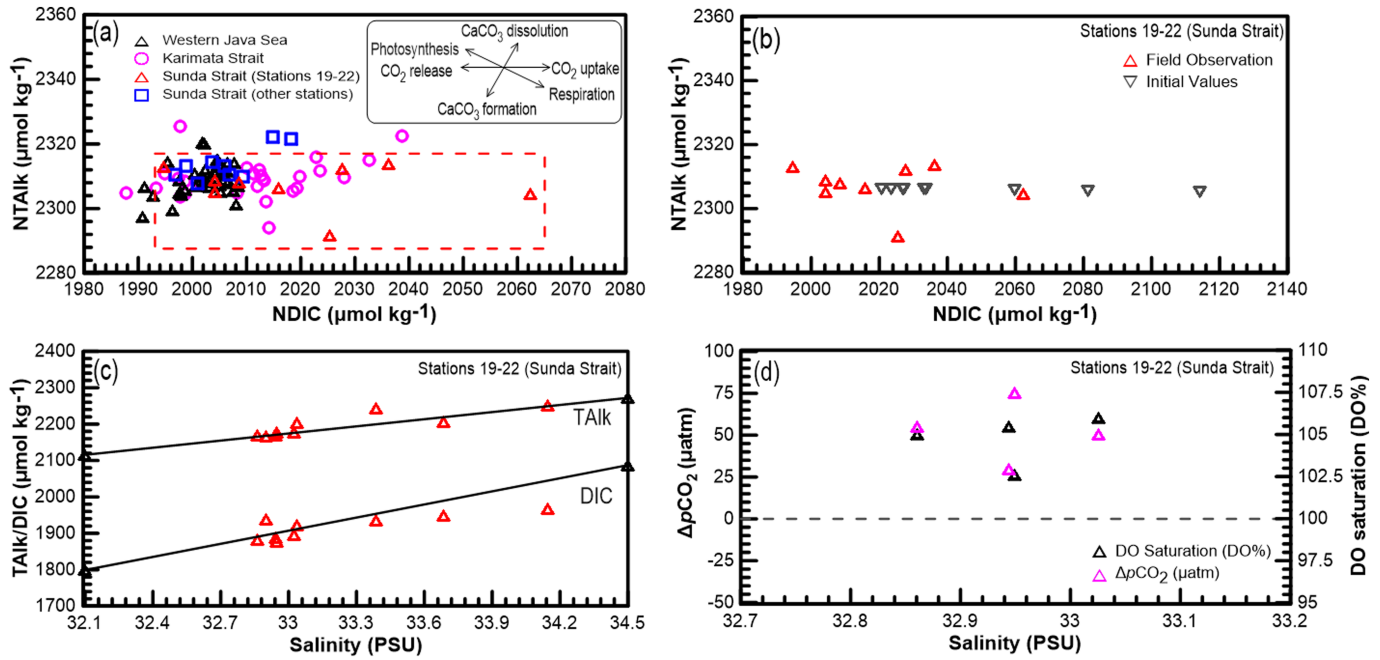


Figure 11. Relationship between NTalk and NDIC (Deffeyes diagram) in the upper 40 m of (a) the entire study area and (b) stations 19 to 22 in the Sunda Strait. (c) TALK and DIC versus salinity in the upper 40 m of stations 19 to 22 in the Sunda Strait. (d) Sea-air $p\text{CO}_2$ difference ($\Delta p\text{CO}_2 = p\text{CO}_2^{\text{seawater}} - p\text{CO}_2^{\text{air}}$) and dissolved oxygen saturation (DO%) in the very surface water of stations 19 to 22 in the Sunda Strait. The inset in panel (a) indicates theoretical distribution patterns for various physical and biogeochemical processes affecting NTalk and NDIC. In panel (b), grey triangles denote the initial NTalk and NDIC of the source water for each field sample, which were calculated based on a two end-member mixing scheme shown in panel (c). The dashed line in panel (d) indicates $\Delta p\text{CO}_2 = 0$ and $\text{DO}\% = 100\%$ with equilibrium reached between the sea surface and the atmosphere. DIC, dissolved inorganic carbon; NDIC, normalized dissolved inorganic carbon; TALK, total alkalinity; NTalk, normalized total alkalinity; PSU, practical salinity unit.

$$\text{DIC}^{\text{cons}} = \frac{\text{Sal}^{\text{meas}}}{\text{Sal}^{\text{ref}}} \times \text{DIC}^{\text{ref}}, \quad (5)$$

$$\text{TALK}^{\text{cons}} = \frac{\text{Sal}^{\text{meas}}}{\text{Sal}^{\text{ref}}} \times \text{TALK}^{\text{ref}}, \quad (6)$$

Sal^{meas} is the measured salinity. Sal^{ref} , DIC^{ref} , and TALK^{ref} are the salinity, DIC, and TALK concentration references in waters beneath the surface mixed layer depth (20 to 48 m).

ΔDIC is thus the difference between DIC^{cons} and measured DIC values (DIC^{meas}):

$$\Delta\text{DIC} = \text{DIC}^{\text{cons}} - \text{DIC}^{\text{meas}}. \quad (7)$$

Positive ΔDIC values indicate net removal and negative values suggest net addition of DIC.

In addition to release into the atmosphere through air-sea gas exchange, DIC can also be removed through biological consumption stimulated by the nutrients associated with large riverine plumes from the Kapuas River and other rivers surrounding the western Indonesian Seas. In the Karimata Strait, however, we found the DIC uptake was minor, while physical mixing was the dominant process. This is supported by the tight linear relationship between DIC and salinity (Figure 9c, DIC vs. salinity) with a correlation coefficient r^2 of 0.93. Consistently, DO saturation (the measured DO divided by the DO concentration at equilibrium with the atmosphere or DO%) in the region was near equilibrium to the atmosphere (98–106%, Figure 12c, Karimata Strait), indicating that its dynamics were mainly controlled by other factors than biological production. Similar process also features the western Java Sea where all DIC data points collected in the surface mixed layer were aligned with the mixing line (Figure 9c, DIC vs. salinity, $r^2 = 0.84$), suggesting again that physical mixing dominated over biological activities.

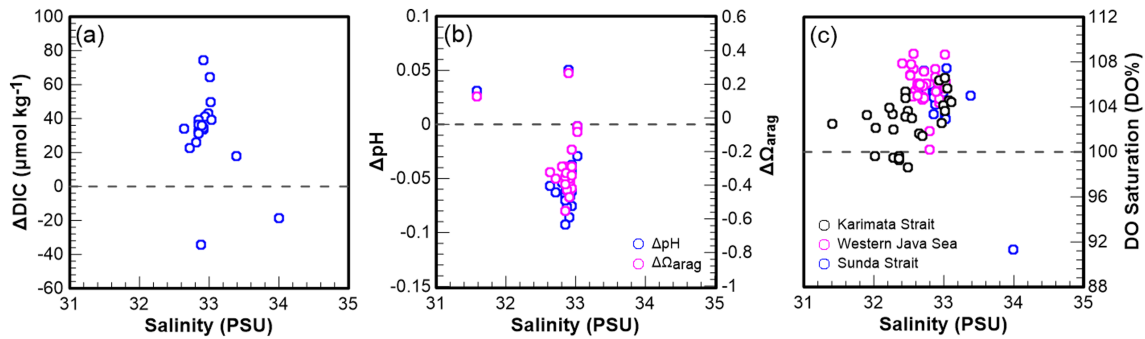


Figure 12. Biologically mediated DIC variations represented by ΔDIC ($\Delta\text{DIC} = \text{DIC}^{\text{cons}} - \text{DIC}^{\text{meas}}$) (a) and ΔpH ($\Delta\text{pH} = \text{pH}^{\text{cons}} - \text{pH}^{\text{meas}}$) and $\Delta\Omega_{\text{arag}}$ ($\Delta\Omega_{\text{arag}} = \Omega_{\text{arag}}^{\text{cons}} - \Omega_{\text{arag}}^{\text{meas}}$) (b) in the surface mixed layer (upper 40 m) of the Sunda Strait. (c) Dissolved oxygen saturation (DO%) in the upper 40 m of the western Indonesian Seas during the southeast monsoon of June 2015. DIC^{cons} is calculated according to equation (5), while pH^{cons} and $\Omega_{\text{arag}}^{\text{cons}}$ are calculated by applying DIC^{cons} and $\text{TALK}^{\text{cons}}$ (equation (6)) into the CO_2SYS program (Lewis & Wallace, 1998). Grey dashed lines in panels (a) and (b) denote no net change in ΔDIC , ΔpH , and $\Delta\Omega_{\text{arag}}$ due to equal amounts of addition and removal, and in panel (c) denotes $\text{DO}\% = 100\%$ with equilibrium reached between the sea surface and the atmosphere. DIC, dissolved inorganic carbon.

In the Sunda Strait, the removal of DIC was significant in the surface mixed layer and ΔDIC (equation (7)) ranged from 18 to 74 $\mu\text{mol kg}^{-1}$ with an average of $31 \pm 23 \mu\text{mol kg}^{-1}$ (Figure 12a). This is attributed to enhanced biological consumption stimulated by rich nutrient supply via water displacement in the western Indonesian Seas, which is generated by westward wind stress persistently pushing waters from the Java Sea into the Indian Ocean via the Sunda Strait (blue pathway in Figure 1b; Susanto et al., 2016). Indeed, high chlorophyll-a induced by nutrient-rich water was previously reported in the Sunda Strait during the southeast monsoon season (Xu et al., 2018). The net removal of DIC appears diminished at high salinities (>33.5 PSU) in the Sunda Strait. On the other hand, a few negative values of ΔDIC at a relatively low salinity of ~ 32.8 PSU (depth = 38 m) in the Sunda Strait indicated a DIC addition of $\sim 18 \mu\text{mol kg}^{-1}$, coinciding with slight undersaturation of DO ($\sim 91\%$), likely resulting from the remineralization of particulate organic matter. Furthermore, during the southeast monsoon, plume-derived nutrients from the JSW continuously stimulate biological production and thus DIC removal, which should be later accompanied by the addition of DIC via the particulate organic matter degradation near bottom-flowing subsurface water. During the present survey, however, we observed that in the subsurface water at 50–100 m, DIC, rather than being added, was overall consumed (on average $54 \pm 45 \mu\text{mol kg}^{-1}$) via organic carbon production during bottom water transport from the Indian Ocean to the northern Sunda Strait, likely associated with upwelling (Wei et al., 2019; Xu et al., 2018). Note that here we selected two water masses at 40 and 150 m, respectively, to construct a two end-member mixing scheme and estimate the deviation of DIC from the conservative mixing control.

Along with the DIC drawdown and DO enhancement, we also observed an increase in Ω_{arag} and pH in the surface mixed layer of the Sunda Strait. To quantify biologically mediated changes in pH and Ω_{arag} , we calculated ΔpH and $\Delta\Omega_{\text{arag}}$ in a similar way as that for ΔDIC (i.e., $\Delta\text{pH} = \text{pH}^{\text{cons}} - \text{pH}^{\text{meas}}$ and $\Delta\Omega_{\text{arag}} = \Omega_{\text{arag}}^{\text{cons}} - \Omega_{\text{arag}}^{\text{meas}}$; pH^{cons} and $\Omega_{\text{arag}}^{\text{cons}}$ denote mixing-predicted pH and Ω_{arag} and are calculated by applying DIC^{cons} (equation (5)) and $\text{TALK}^{\text{cons}}$ (equation (6)) into the CO_2SYS program (Lewis & Wallace, 1998). Positive values of ΔpH and $\Delta\Omega_{\text{arag}}$ indicate net addition and their negative values suggest net removal of DIC.

Both $\Delta\Omega_{\text{arag}}$ and ΔpH had an opposite pattern to that of ΔDIC , with the former ranged between -0.55 to 0.26 and the latter ranged between -0.09 to 0.05 (Figure 12b). The majority of ΔpH and $\Delta\Omega_{\text{arag}}$ values are negative, indicating significant DIC removal or net primary production leading to the increase in pH and Ω_{arag} . This process would potentially counter the effect of ocean acidification via anthropogenic CO_2 invasion in the surface mixed layer of the Sunda Strait. As a consequence, we suggest that high freshwater discharge and associated nutrients from rivers to the western Indonesian Seas, as well as strong monsoon-driven water circulation, may enhance primary productivity and stimulate DIC consumption, which result in an increase in Ω_{arag} and pH in the surface mixed layer.

5. Concluding Remarks

Here we have examined the dynamics of the carbonate system in the western Indonesian Seas during the southeast monsoon. By observing water mass characteristics, we demonstrated that low salinity waters originating from the Kapuas River plume (in Kalimantan) mixed with Java Sea-SCS water as well as subsurface Indian Ocean water, resulting in homogeneous distributions of salinity and temperature. Based on water mass structures and properties, we have identified the Sunda Strait as one of the main outflows of the ITF in western Indonesia.

Concentrations of DIC and TALK were low in the shallow river plume in the Karimata Strait and homogeneous in the western-most region of the Java Sea. While physical processes and air-sea gas exchange exerted large controls on the carbonate dynamics in the entire area under study, significant DIC removal associated with biological production was observed in the upper and subsurface Sunda Strait. The western Indonesian Seas acted as a source of CO₂ to the atmosphere with an average net degassing flux of 2.98 mmol C m⁻² day⁻¹. It must be noted that the controlling processes of the carbonate system in this undersampled region may vary temporally, both over seasonal and interannual scales which have not been fully resolved.

Acknowledgments

Faisal Hamzah acknowledges the China Marine Government Scholarship for providing the funding during his study at Xiamen University (2014SOA003 and 2017SOA016125). This work was funded by the China National Science Foundation through Grants 41730533 and 41890804, the National Key Scientific Research Project through Grant 2015CB954001 (Minhan Dai), DIPA of Ministry of Marine Affairs and Fisheries 2015, Indonesia (Teguh Agustadi), Grant N00014-08-01-0618 of The Office of Naval Research and Grant #OCE-07-25935 of the National Science Foundation, USA (R. Dwi Susanto), and Grant 41476025 and 41506036 of the National Science Foundation of China (Zexun Wei). We thank “The Southeast China Sea- Indonesian seas Transport/Exchange (SITE) and Dynamics of Sunda and Lombok Straits, and Their Impacts on Seasonal Fish Migration” program, and joint research between Indonesia, China, and the United States for the opportunity for the sampling cruise. We would like to thank the captain and crews of the *R/V Baruna Jaya VIII* of the Indonesian Institute of Science for their help and cooperation during the cruise. Yan Li provided significant assistance during sample preparation and analysis. We thank Elliott G. Roberts and Wei Yang for constructive discussion and two anonymous reviewers for insightful comments. The authors declare that the main data supporting the findings of this study are archived and can be retrieved at PANGAEA (<https://doi.pangaea.de/10.1594/PANGAEA.908458>).

References

- Afdal, R., Kaswadji, F., & Koropitan, A. F. (2012). Air-sea CO₂ exchange in the Nasik Strait water, Belitung. *Journal of Segara*, 8(1), 9–17. (In Bahasa)
- Aldrian, E., & Susanto, R. D. (2003). Identification of three dominant rainfall regions within Indonesia and their relationship to sea surface temperature. *International Journal of Climatology*, 23, 1435–1452. <https://doi.org/10.1002/joc.950>
- Atmadipoera, A., Molcard, R., Madec, G., Wijffels, S., Sprintall, J., Koch-Larrouy, A., et al. (2009). Characteristics and variability of the Indonesian throughflow water at the outflow straits. *Deep Sea Research Part I*, 56(11), 1942–1954. <https://doi.org/10.1016/j.dsr.2009.06.004>
- Baker, A. C., Glynn, P. W., & Riegl, B. (2008). Climate change and coral reef bleaching: An ecological assessment of long-term impacts, recovery trends and future outlook. *Estuary, Coastal and Shelf Science*, 80(4), 435–471. <https://doi.org/10.1016/j.ecss.2008.09.003>
- Bates, N. R., Pequignat, A. C., & Sabine, C. L. (2006). Ocean carbon cycling in the Indian Ocean: 1. Spatiotemporal variability of inorganic carbon and air–sea CO₂ gas exchange. *Global Biogeochemical Cycles*, 20, GB3020. <https://doi.org/10.1029/2005GB002491>
- Broecker, W. S. (1991). The great ocean conveyor. *Oceanography*, 4, 79–89. <https://doi.org/10.5670/oceanog.1991.07>
- Cao, Z., Dai, M., Zheng, N., Wang, D., Li, Q., Zhai, W., et al. (2011). Dynamics of the carbonate system in a large continental shelf system under the influence of both a river plume and coastal upwelling. *Journal of Geophysical Research*, 116, G02010. <https://doi.org/10.1029/2010JG001596>
- Cao, Z., Yang, W., Zhao, Y., Guo, X., Yin, Z., Du, C., et al. (2019). Diagnosis of CO₂ dynamics and fluxes in global coastal oceans. *National Science Review*, nzw105. <https://doi.org/10.1093/nsr/nwz105>
- Chen, C. T. C. (2002). Shelf-vs. dissolution-generated alkalinity above the chemical lysocline. *Deep Sea Research Part II*, 49(24–25), 5365–5375. [https://doi.org/10.1016/S0967-0645\(02\)00196-0](https://doi.org/10.1016/S0967-0645(02)00196-0)
- Chen, C. T. C., Hou, W.-P., Gamo, T., & Wang, S. H. (2006). Carbonate-related parameters of subsurface waters in the West Philippine, South China and Sulu Seas. *Marine Chemistry*, 99, 151–161. <https://doi.org/10.1016/j.marchem.2005.05.008>
- Chen, C. T. C., & Millero, F. J. (1979). Gradual increase of oceanic CO₂. *Nature*, 277, 205–206. <https://doi.org/10.1038/277205a0>
- Chen, C. T. C., & Pytkowicz, R. M. (1979). On the total CO₂-titration alkalinity oxygen system in the Pacific Ocean. *Nature*, 281(5730), 362–365. <https://doi.org/10.1038/281362a0>
- Chen, C. T. C., Wang, S.-L., Chou, W.-C., & Sheu, D. D. (2006). Carbonate chemistry and projected future changes in pH and CaCO₃ saturation state of the South China Sea. *Marine Chemistry*, 101, 277–305. <https://doi.org/10.1016/j.marchem.2006.01.007>
- Dai, M., Cao, Z., Guo, X., Zhai, W., Liu, Z., Yin, Z., et al. (2013). Why are some marginal seas sources of atmospheric CO₂? *Geophysical Research Letters*, 40, 2154–2158. <https://doi.org/10.1002/grl.50390>
- Dickson, A. G., & Millero, F. J. (1987). A comparison of the equilibrium constants for the dissociation of carbonic acid in seawater media. *Deep Sea Research, Part I*, 34, 1733–1743. [https://doi.org/10.1016/0198-0149\(87\)90021-5](https://doi.org/10.1016/0198-0149(87)90021-5)
- Dickson, A. G., Sabine, C. L., & Christian, J. R. (Eds) (2007). Guide to best practices for ocean CO₂ measurements. (PICES special publication 3, pp 191). Retrieved from Ocean Best Practices. <http://hdl.handle.net/11329/249>.
- Fang, G., Susanto, R. D., Wirasantosa, S., Qiao, F., Supangat, A., Fan, B., et al. (2010). Volume, heat, and freshwater transports from the South China Sea to Indonesian seas in the boreal winter of 2007–2008. *Journal of Geophysical Research*, 115, C12020. <https://doi.org/10.1029/2010JC006225>
- Ferrera, C. M., Jacinto, G. S., Chen, C. T. C., Diego-McGlone, M. L., Datoc, M. F. K. T., et al. (2017). Carbonate parameters in high and low productivity areas of the Sulu Sea. *Philippines. Mar. Chem.*, 195, 2–14. <https://doi.org/10.1016/j.marchem.2017.08.005>
- Gordon, A. L. (1986). Inter-ocean exchange of thermohaline water. *Journal of Geophysical Research*, 91(C4), 5037–5046. <https://doi.org/10.1029/JC091iC04p05037>
- Gordon, A. L. (2005). Oceanography of the Indonesian seas and their throughflow. *Oceanography*, 18, 14–27. <https://doi.org/10.5670/oceanog.2005.01>
- Gordon, A. L., Susanto, R. D., & Vranes, K. (2003). Cool Indonesian throughflow as a consequence of restricted surface layer flow. *Nature*, 425(6960), 824–828. <https://doi.org/10.1038/nature02038>
- Guo, X., & Wong, G. T. F. (2015). Carbonate chemistry in the Northern South China Sea Shelf-sea in June 2010. *Deep Sea Research Part II*, 117, 119–130. <https://doi.org/10.1016/j.dsr2.2015.02.024>
- He, Z., Feng, M., Wang, D., & Slawinski, D. (2015). Contribution of the Karimata Strait transport to the Indonesian throughflow as seen from a data assimilation model. *Continental Shelf Research*, 92, 16–22. <https://doi.org/10.1016/j.csr.2014.10.007>

- Hendiarti, N., Aldrian, E., Amri, K., Andiajstuti, R., Sachoemar, S. I., & Wahyono, I. B. (2005). Seasonal variation of pelagic fish catch around Java. *Oceanography*, *18*(4), 112–123. <https://doi.org/10.5670/oceanog.2005.12>
- Hendiarti, N., Siegel, H., & Ohde, T. (2002). Distinction of different water masses in and around the Sunda Strait: Satellite observations and in-situ measurements. In *Paper presented at 6th Pan Ocean Remote Sensing Conference (PORSEC)* (pp. 674–679). Bali: Indonesia.
- Hendiarti, N., Siegel, H., & Ohde, T. (2004). Investigation of different coastal processes in Indonesian waters using SeaWiFS data. *Deep Sea Research Part II*, *51*(1-3), 85–97. <https://doi.org/10.1016/j.dsr2.2003.10.003>
- Hirst, A. C., & Godfrey, J. S. (1993). The role of Indonesian throughflow in a global ocean GCM. *Journal of Physical Oceanography*, *23*, 1057–1086. [https://doi.org/10.1175/1520-0485\(1993\)023<1057:TROITI>2.0.CO;2](https://doi.org/10.1175/1520-0485(1993)023<1057:TROITI>2.0.CO;2)
- Ho, D. T., Law, C. S., Smith, M. J., Schlosser, P., Harvey, M., & Hill, P. (2006). Measurements of air-sea gas exchange at high wind speeds in the Southern Ocean: Implications for global parameterizations. *Geophysical Research Letters*, *33*(16), L16611. <https://doi.org/10.1029/2006GL026817>
- Ilyina, T., Zeebe, R. E., Maier-Reimer, E., & Heinze, C. (2009). Early detection of ocean acidification effects on marine calcification. *Global Biogeochemical Cycles*, *23*, GB1008. <https://doi.org/10.1029/2008GB003278>
- Jiang, Z. P., Huang, J. C., Dai, M., Kao, S. J., Hydes, D. J., Chou, W. C., & Jan, S. (2011). Short-term dynamics of oxygen and carbon in productive nearshore shallow seawater systems off Taiwan: Observations and modeling. *Limnology and Oceanography*, *56*(11), 1832–1849. <https://doi.org/10.4319/lo.2011.56.5.1832>
- Jiang, Z.-P., Tyrrell, T., Hydes, D. J., Dai, M., & Hartman, S. E. (2014). Variability of alkalinity and the alkalinity-salinity relationship in the tropical and subtropical surface ocean. *Global Biogeochemical Cycles*, *28*, 729–742. <https://doi.org/10.1002/2013GB004678>
- Johnson, K. M., Dickson, A. G., Eiseheid, G., Goyet, C., Guenther, P. R., Key, R. M., et al. (2002). In A. Kozyr (Ed.), *Carbon Dioxide, hydrographic and chemical data obtained during the nine R/V Knorr cruises comprising the Indian Ocean CO₂ Survey (WOCE Sections 18S19S, 19N, 18N15E, 13, 15W14, 17N, 11, 110, and 12; December 1, 1994–January 22, 1996)*. Oak Ridge, Tennessee: ORNL/CDIAC-138, NDP-080. Carbon Dioxide Information Analysis Center, Oak Ridge National Laboratory, U.S. Department of Energy. <https://doi.org/10.3334/CDIAC/otg.ndp080>, https://www.nodc.noaa.gov/ocads/oceans/woce_i10.html
- Kartadikaria, A. R., Watanabe, A., Nadaoka, K., Adi, N. S., Prayitno, H. B., Soemurumekso, S., et al. (2015). CO₂ sink/source characteristics in the tropical Indonesian seas. *Journal of Geophysical Research: Oceans*, *120*, 7842–7856. <https://doi.org/10.1002/2015JC010925>
- Kästner, K., Hoitink, A. J. F., Torfs, P. J. J. F., Vermeulen, B., Ningsih, N. S., & Pramulya, M. (2018). Prerequisites for accurate monitoring of river discharge based on fixed-location velocity measurements. *Water Resources Research*, *54*, 1058–1076. <https://doi.org/10.1002/2017WR020990>
- Labasque, T., Chaumery, C., Aminot, A., & Kergoat, G. (2004). Spectrophotometric Winkler determination of dissolved oxygen: Re-examination of critical factors and reability. *Marine Chemistry*, *88*, 53–60. <https://doi.org/10.1016/j.marchem.2004.03.004>
- Lewis, E., & Wallace, D. W. R. (1998). *Program developed for CO₂ system calculations, ORNL/CDIAC-105, carbon dioxide Inf, Anal. Cent., Oak Ridge Natl. Lab., U.S* (p. 38 pp. Retrieved from). Oak Ridge, Tenn: Dep. of Energy. <https://salish-sea.pnnl.gov/media/ORNL-CDIAC-105.pdf>
- Li, S., Wei, Z., Susanto, R. D., Zhu, Y., Setiawan, A., Xu, T., et al. (2018). Observations of intraseasonal variability in the Sunda Strait throughflow. *Journal of Oceanography*, *74*(5), 541–547. <https://doi.org/10.1007/s10872-018-0476-y>
- Mehrbach, C., Culbertson, C. H., Hawley, J. E., & Pytkowicz, R. M. (1973). Measurement of the apparent dissociation constants of carbonic acid in seawater at atmospheric pressure. *Limnology and Oceanography*, *18*, 897–907. <https://doi.org/10.4319/lo.1973.18.6.0897>
- Pai, S.-C., Gong, G.-C., & Liu, K.-K. (1993). Determination of dissolved oxygen in seawater by direct spectrophotometry of total iodine. *Marine Chemistry*, *41*, 343–351. [https://doi.org/10.1016/0304-4203\(93\)90266-Q](https://doi.org/10.1016/0304-4203(93)90266-Q)
- Potemra, J. T., Hacker, P. W., Melnichenko, O., & Maximenko, N. (2016). Satellite estimate of freshwater exchange between the Indonesian seas and the Indian Ocean via the Sunda Strait. *Journal of Geophysical Research: Oceans*, *121*, 5098–5111. <https://doi.org/10.1002/2015JC011618>
- Putri, M. R. (2005). *Study of ocean climate variability (1959–2002) in the eastern Indian Ocean, Java Sea and Sunda Strait using the HAMBURG Shelf Ocean Model. (Doctoral Dissertation)* (p. 104). Hamburg, Germany: Univ. Hamburg. pp
- Saji, N. H., Goswami, B. N., Vinayachandran, P. N., & Yamagata, T. (1999). A dipole mode in the tropical Indian Ocean. *Nature*, *401*, 360–363. <https://doi.org/10.1038/43854>
- Schlitzer, R. (2018). Ocean data view. <https://odv.awi.de>
- Schneider, N. (1998). The Indonesian throughflow and the global climate system. *Journal of Climate*, *11*(4), 676–689. [https://doi.org/10.1175/1520-0442\(1998\)011<0676:TITATG>2.0.CO;2](https://doi.org/10.1175/1520-0442(1998)011<0676:TITATG>2.0.CO;2)
- Setiawan, R. Y., Mohtadi, M., Southon, J., Groeneveld, J., Steinke, S., & Hebbeln, D. (2015). The consequences of opening the Sunda Strait on the hydrography of the eastern tropical Indian Ocean. *Paleoceanography*, *30*, 1358–1372. <https://doi.org/10.1002/2015PA002802>
- Sprintall, J., Gordon, A. L., Koch-Larrouy, A., Lee, T., Potemra, J. T., Pujiana, K., & Wijffels, S. E. (2014). The Indonesian seas and their role in the coupled ocean-climate system. *Nature Geoscience*, *7*, 487–492. <https://doi.org/10.1038/NCEO2188>
- Susanto, R. D., Fang, G., Soesilo, I., Zheng, Q., Qiao, F., Wei, Z., & Sulisty, B. (2010). New surveys of a branch of the Indonesian throughflow. *EOS Trans. AGU*, *91*(30). <https://doi.org/10.1029/2010EO300002>
- Susanto, R. D., Gordon, A. L., & Zheng, Q. (2001). Upwelling along the coasts of Java and Sumatra and its relation to ENSO. *Geophysical Research Letters*, *28*, 1599–1602. <https://doi.org/10.1029/2000GL011844>
- Susanto, R. D., & Marra, J. (2005). Effect of the 1997/98 El Niño on chlorophyll a variability along the southern coasts of Java and Sumatra. *Oceanography*, *18*(4), 124–127. <https://doi.org/10.5670/oceanog.2005.13>
- Susanto, R. D., Moore II, T. S., & Marra, J. (2006). Ocean color variability in the Indonesian seas during the SeaWiFS era. *Geochemistry, Geophysics, Geosystems*, *7*, Q05021. <https://doi.org/10.1029/2005GC001009>
- Susanto, R. D., Wei, Z., Adi, R. T., Fan, B., Li, S., & Fang, G. (2013). Observation of the Karimata Strait throughflow from December 2007 to November 2008. *Acta Oceanologica Sinica*, *32*(5), 1–6. <https://doi.org/10.1007/s13131-013-0307-3>
- Susanto, R. D., Wei, Z., Adi, T. R., Zheng, Q., Fang, G., Fan, B., et al. (2016). Oceanography surrounding Krakatau Volcano in the Sunda Strait, Indonesia. *Oceanography*, *29*(2), 264–272. <https://doi.org/10.5670/oceanog.2016.31>
- Sweeney, C., Gloor, E., Jacobson, A. R., Key, R. M., McKinley, G., Sarmiento, J. L., et al. (2007). Constraining global air-sea gas exchange for CO₂ with recent bomb ¹⁴C measurements. *Global Biogeochemical Cycles*, *21*, GB2015. <https://doi.org/10.1029/2006GB002784>
- Tranchant, B., Reffray, G., Greiner, E., Nugroho, D., Koch-Larrouy, A., & Gaspar, P. (2016). Evaluation of an operational ocean model configuration at 1/12° spatial resolution for the Indonesian seas (NEMO2.3/INDO12)-Part 1: Ocean physics. *Geoscientific Model Development*, *9*, 1037–1064. <https://doi.org/10.5194/gmd-9-1037-2016>
- Tseng, C.-M., Wong, G. T. F., Chou, W.-C., Lee, B.-S., Sheu, D.-D., & Liu, K.-K. (2007). Temporal variations in the carbonate system in the upper layer at the SEATS station. *Deep Sea Research Part II*, *54*, 1448–1468. <https://doi.org/10.1016/j.dsr2.2007.05.003>

- Tun, K., Chou, L. M., Cabanban, A., Tuan, V. S., Philreefs, Y., Suharsono, T. Y., et al. (2004). Status of coral reefs, coral reef monitoring and management in Southeast Asia, 2004. In C. R. Wilkinson (Ed.), *Status of coral reefs of the world: 2004* (Vol. 1, pp. 235–275). Townsville: Australian Institute of Marine Science.
- Wajsowicz, R. C., & Schneider, E. K. (2001). The Indonesian throughflow's effect on global climate determined from the COLA coupled climate system. *Journal of Climate*, *14*, 3029–3042. [https://doi.org/10.1175/1520-0442\(2001\)014<3029:TITSEO>2.0.CO;2](https://doi.org/10.1175/1520-0442(2001)014<3029:TITSEO>2.0.CO;2)
- Wang, Y., Xu, T., Li, S., Susanto, R. D., Sulisty, B., Supangat, A., et al. (2019). Seasonal variation of the water transport through the Karimata Strait. *Acta Oceanologica Sinica, Acta Oceanologica Sinica*, *38*(4), 47–57. <https://doi.org/10.1007/s13131-018-1224-2>
- Wanninkhof, R. (1992). Relationship between wind speed and gas exchange over the ocean. *Journal of Geophysical Research*, *97*(C5), 7373–7382. <https://doi.org/10.1029/92JC00188>
- Wei, Z., Li, S., Susanto, R. D., Wang, Y., Fan, B., Xu, T., et al. (2019). An overview of 10-year observation of the South China Sea branch of the Pacific to Indian Ocean throughflow at the Karimata Strait. *Acta Oceanologica Sinica*, *38*(4), 1–11. <https://doi.org/10.1007/s13131-019-1410-x>
- Weiss, R. F. (1974). Carbon dioxide in water and seawater: The solubility of a non-ideal gas. *Marine Chemistry*, *2*(3), 203–215. [https://doi.org/10.1016/0304-4203\(74\)90015-2](https://doi.org/10.1016/0304-4203(74)90015-2)
- Weiss, R. F., & Price, B. A. (1980). Nitrous oxide solubility in water and seawater. *Marine Chemistry*, *8*(4), 347–359. [https://doi.org/10.1016/0304-4203\(80\)90024-9](https://doi.org/10.1016/0304-4203(80)90024-9)
- Wijffels, S. E., Schmitt, R. W., Bryden, H. L., & Stigerbrandt, A. (1992). Transport of freshwater by the oceans. *Journal of Physical Oceanography*, *22*, 155–162. [https://doi.org/10.1175/1520-0485\(1992\)022<0155:TOFBTO>2.0.CO;2](https://doi.org/10.1175/1520-0485(1992)022<0155:TOFBTO>2.0.CO;2)
- Wyrtki, K. (1961). Scientific results of marine investigations of the South China Sea and the Gulf of Thailand. In *Naga Report*, 2. Scripps Institute of Oceanography, La Jolla, California: University of California, 1959–1961.
- Xu, T., Li, S., Hamzah, F., Setiawan, A., Susanto, R. D., Cao, G., et al. (2018). Intraseasonal flow and its impact on the chlorophyll-a concentration in the Sunda Strait and its vicinity. *Deep Sea Research Part I*, *136*, 84–90. <https://doi.org/10.1016/j.dsr.2018.04.003>
- Xue, L., Wang, H., Jiang, L-Q., Cai, W.-J., Wei, Q., Song, H., ... Yu, W. (2016). Aragonite saturation state in a monsoonal upwelling system off Java, Indonesia. *Journal of Marine Systems*, *153*, 10–17. <https://doi.org/10.1016/j.jmarsys.2015.08.003>
- Zeebe, R. E., & Wolf-Gladrow, D. (2001). *CO₂ in seawater: Equilibrium, kinetics, isotopes* (Vol. 65, p. 346). Amsterdam: Elsevier Oceanography Series.